DATA DRIVEN APPROACH TO VEHICLE EMISSIONS REDUCTION

A DISSERTATION
SUBMITTED TO THE FACULTY OF
UNIVERSITY OF MINNESOTA
BY

ANDREW JOHN KOTZ

IN PARTIAL FULFILLMENT OF THE REQUIREMENTS
FOR THE DEGREE OF
DOCTOR OF PHILOSOPHY

WILLIAM NORTHROP

DECEMBER 2016

Acknowledgements

I would like to acknowledge Twin Cities Metro Transit for allowing data to be measured from in-service transit buses, installing data logging equipment, and for providing access to bus route information. In particular, I would like to acknowledge David Haas at Metro Transit for his critical assistance in coordinating bus schedules and providing technical guidance on my projects. I would also like to thank Winthrop Watts, Reem Ali and Shashank Singh for their technical contributions, and recognize the University of Minnesota Initiative for Renewable Energy and the Environment (IREE grant RL-0013-13), the University of Minnesota Center for Transportation Studies, the MnDRIVE Robotics scholarship and Cummins for funding my graduate studies.

Thank you to my family for supporting and pushing me for 26 years and to Emily Gross for her inspiration and guidance. I am very fortunate to have them all, and I appreciate everything they have done for me. I would also like to thank Professor Kittelson, Professor Shekhar and Professor Sun for being a part of my thesis committee and advising my throughout my graduate career. Finally, I would like to thank my graduate adviser Professor Northrop for believing in me, encouraging me to pursue new spaces and for pushing me throughout my graduate career. I truly appreciate all of his time and effort put into helping me graduate.

Dedication

I dedicate this thesis to the advancement of science and preservation of our planet.

Abstract

Anthropogenic climate change and air pollution resulting from vehicle emissions are major issues facing society. Recent research and government regulations have focused on reducing these emissions through efficiency improvements, advanced aftertreatment technology and ever-tighter regulations. However, despite these advances vehicles still exhibit high emissions during actual use as compared to laboratory or certification testing.

Using modern data collection techniques, I identified that electrification and hybridization of transit buses can reduce vehicle power consumption by up to 72% under "real-world" driving conditions, thus decreasing vehicle CO_2 emissions. To illustrate the process behind vehicle data collection and offer a use-case for future vehicle connectivity, I discuss the development of a novel mass-based automatic passenger counter to provide a more accurate, lower-cost passenger counting method which can be retrofitted on existing transit buses. Initial results indicate this new passenger counting technology has an accuracy of 97%, however miscounts occur during times when the bus is kneeling, leaving an opportunity for future research.

Using measurements from standard exhaust sensors I revealed that NO_X emissions of 2013 model year (MY) transit buses were 3-9 times the federal test procedure (FTP) certification limit under "real-world" driving conditions while complying with all regulated standards. To help identify the systematic and physical causes for these high NO_X emissions I developed a novel spatial emissions mapping technique called Lagrangian Hotspot Analysis, which used connected vehicle technology to identify spatial influences

on vehicle emissions. Results indicate that a hotspot located in the vicinity of a bus stop and intersection had an emissions rate of roughly 3.3 times that of the route average, with these high emissions being attributed to the long idle periods and slow speeds. Instances of cold start and uphill accelerations were also found to increase NO_X emissions.

Finally, I compared a 2013MY and 2015MY conventional diesel bus to evaluate technology improvements between the generations with the key finding that NO_X emissions from the 2015MY bus are reduced by 80% compared to the 2013MY. Further, the NO_X emissions were lower than the FTP cycle limit under real-world driving. After the 2013MY bus was updated with the emissions aftertreatment technology of the 2015MY bus, I observed the same NO_X reduction in the 2013MY bus. I attribute this reduction to increases in urea consumption through optimization of urea dosing strategy. Such findings imply that certification NO_X levels are possible under real-world driving and that upgrading existing buses with modern aftertreatment systems can provide substantial NO_X reductions.

Table of Contents

List of Tables

List of Figures

Chapter 1 Introduction

Ever mounting evidence of anthropogenic climate change has prompted society to focus efforts on reducing the responsible emissions. The problem affects every individual and living organism on this planet making it a truly global problem requiring many diverse disciplines to solve. According to the 2013 United States Climate Change Report, human activities are the primary cause of the recent rapid increases in mean earth surface temperature resulting from production of heat trapping "greenhouse" gasses (GHG) [1]. Such GHGs include carbon dioxide (CO_2), nitrous oxide (N_2O), methane, and fluorinated gases [2]. Besides GHGs, anthropogenic (human-derived) air pollutants from combustion-powered devices such as oxides of nitrogen (NO_X) that contribute to ground-level ozone chemistry and air quality have damaging effects on humans. The U.S. Environmental Protection Agency (EPA) categorizes the emissions that are detrimental to human health as criteria pollutants. These criteria pollutants include carbon monoxide (CO), lead, nitrogen dioxide (NO_2), tropospheric or ground level ozone, particulate matter and sulfur dioxide [3]. This work focuses on identifying factors that influence real-world production of CO_2 emissions and nitrogen oxide (NO_X) in road vehicles.

Carbon dioxide is the most prevalent GHG on Earth making up 82.5% of all GHGs [4]. The average atmospheric concentration of CO_2 is approximately 400 ppm and is increasing at a rate of 2 ppm per year. This rate has doubled that of the 1960s, where emission rates were around 0.75 ppm per year [5]. Consequences of these harmful emissions include a net warming of the Earth's atmosphere resulting in longer and hotter summers, shorter winters,

more damaging rain storms, higher tides and increased flooding [1]. The U.S. government estimates the current societal cost of releasing one ton of carbon dioxide into the atmosphere to be $21. Yet independent estimates have suggested this cost is severely underestimated and could be closer to $900 per ton of CO_2 released [6]. The economic sectors responsible increasing atmospheric CO_2 concentration are industrial, transportation, commercial, residential and agriculture. Of these, the transportation sector is responsible for 28% of anthropogenic CO_2 [4] implying a small decrease in vehicle emissions would have a large impact on global GHG emissions. Current CO_2 sinks or emission absorbing mechanisms include naturally occurring photosynthesis in forests, absorption by ocean water which is harmful to the ocean, and man-made carbon sequestration. This is not an adequate fix: GHG emissions from energy production are still five times these combined GHG sinks [4,7].

In addition to CO_2, a major focus of this work is to understand factors that influence NO_X production in vehicles powered by internal combustion engines. NO_X consists of NO and NO_2 [8] and is a precursor to tropospheric ozone [9,10]. When inhaled at low concentrations over extended time periods, the NO_2 compound of NO_X can restrict breathing, inflame airways, and make lungs more susceptible to infection [11]. Common health risks associated with NO_X exposure include respiratory inflammation for healthy people and increased health issues for those with asthma [12].

Emissions regulations have been put in place to reduce harmful pollutants from entering the Earth's atmosphere with the intent of reducing climate change and/or

increasing air quality [13]. The U.S. government has attempted to enforce this change by enacting Corporate Average Fuel Economy (CAFE) standards requiring rolling increases in fleet average fuel economy to achieve 52.4 miles per gallon (MPG) by 2025. Although the regulations are stringent, the actual fuel economy that vehicles achieve on U.S. roads is drastically different from their regulated values. The U.S. EPA states that real-world fuel economy can be on average 25% less than CAFE standards [14]. Using a simple calculation of distribution of vehicles on the road in 2011 [15] and the regulated "sticker" mileage of those vehicles [16], the yearly fleet average fuel economy should have been 32 MPG. Yet dividing the U.S. Department of Transportation reported miles traveled [17] by total gallons of fuel consumed [18] resulted in an actual average 2011 U.S. fleet fuel economy of 22 MPG [18,19]. Many have shown that emissions observed in practice are far higher than mandated despite government mandates requiring vehicles and engines to meet these standards when certified in a laboratory. Such studies demonstrate and motivate the importance of real-world testing to understand and quantify the effects of unforeseen environmental variables on vehicle emissions.

Not only does in-use fuel economy differ from regulated standards, pollutant emissions in real-world driving are also higher. A study by Wu et al. showed that real-world heavy-duty NO_X emissions were substantially higher than laboratory certifications [20]. Similarly, a study in China showed that real-world fuel consumption was 15% higher than sticker values [21]. A study by Boriboonsomsin et al. showed that road grade can reduce fuel economy by up to 20% suggesting that a flatter, longer route could potentially increase fuel

economy [22]. Another study involving heavy-duty diesel trucks found that about 33% of operation was spent idling the engine, thus contributing to the relatively poor fuel economy of trucks in this segment [23]. Low-load driving at slow speeds has been shown to produce elevated NO_X emissions in model year 2010 heavy-duty diesel engines despite being equipped with selective catalytic reduction (SCR) devices for reducing NO_X emissions [24]. Aggressive driving behaviors have been shown to reduce hybrid vehicle fuel economy by over 30% [25]. Such exogenous variables contribute significantly to vehicle emissions. Barth et al. tried to capture these real-world effects by deriving an equation for CO_2 emissions based solely on average trip velocity. Analysis of a dataset containing over 15,000 entries showed that real-world traffic conditions can increase CO_2 emissions by 12% [26].

This divergence is generally not a result of the vehicles functioning outside of their designed operating conditions or failing certification tests. It is emblematic of a systematic flaw in the vehicle certification process whereby the tests do not accurately reflect how vehicles are operated in the real-world. Current certification testing procedures are microscopic examinations of a vehicle's performance on a test cycle designed to represent a lifetime of use. While ideally sound, this method fails to account for macroscopic conditions encountered in day-to-day driving and neglects the intimate spatiotemporal network connections a vehicle's emissions has to climate, road and traffic conditions. These real-world studies provide invaluable insight into the macroscopic interactions of vehicles and their environment with the key limitation being dataset size and scalability. The aforementioned study by Barth et al. involved about 4 hours of vehicle data from the

Los Angeles metro area [26], and the study by Boriboonsomsin et al. evaluated approximately 1,300 heavy-duty diesel trucks from California [23]. While this research is very meaningful, it fails to account for the diverse locations and driving conditions that constitute the entire spectrum of vehicle to environment interactions. This is likely due to the costly resources required to capture such information [23] and relatively manual methods for analyzing the data. Furthermore, the evolution of onboard diagnostics (OBD) systems and emissions regulations requiring all vehicles to have OBD has enabled access to thousands of standard vehicle operating parameters, with more sensors being added every year [27]. Auto manufacturer Audi has even added sensors to indicate when the vehicle's engine motor mounts are failing [28], and Ford has developed an open data exchange called OpenXC for customers to access their vehicle's data [29]. Additionally, the U.S. DOT has announced it will begin taking steps towards implementing vehicle-to-vehicle (V2V), vehicle-to-infrastructure (V2I) and vehicle-to-everything (V2X) communication for all light duty vehicles in the near future [30], making connection to vehicle data a much more viable option.

Understanding real-world vehicle behavior is a multifaceted problem not achievable using a unidisciplinary approach. One key challenge of V2X concepts is the potentially immense amount of data that may need to be analyzed. For example, if 100 variables were collected from the over 250 million vehicles registered in the U.S. [19]on a second-by-second basis for one day, the dataset would contain over 90 trillion entries. The sheer volume of obtainable geo-located OBD parameters makes amounts to a "Spatial Big Data" problem. Spatial Big Data (SBD) analytics is a rapidly growing research subset of the computer

science field dedicated to interpreting large datasets linked through multiple spatial dimensions. Such studies lend themselves to large-scale vehicle research, an approach which has had notable successes, including UPS's implementation to avoid left turns saving millions of gallons of fuel [31]. This realization was estimated to have saved UPS $30 million, prompting the company to attempt using these analytics to optimize their aircraft fleet [32]. A new paradigm of vehicle research utilizing SBD Analytics is necessary to obtain meaningful results from this vast amount of possible data. Many industries have benefited from traditional Big Data analytics. Businesses use big data analytics on point-of-sale transaction data to provide target marketing or prevent fraud with great success, and molecular biology researchers are applying these techniques to genomic data to understand the structure and function of genes [33]. The database systems and data analytics used for these purposes, however, lack the functionality to represent and perform computations in multiple dimensions. A spatial database management system and SBD analytics are required to address the spatial autocorrelation of vehicle data [34].

Spatial computing techniques have been used with great success in traffic studies and vehicle routing to minimize travel time or route vehicles around congested areas [35–37]. Executing these queries first requires an understanding of what traffic conditions exist. This is accomplished by identifying spatial road segments with high traffic densities or clusters of slow moving vehicles using hotspot recognition [38,39]. Spatial outlier recognition and anomaly detection have been used to look for anomalous traffic patterns or traffic accidents using roadway loop detector data [40,41]. Such methods can be adapted to detect

instances of elevated vehicle emissions or anomalous vehicle operation preceding a malfunction.

In this work I examine emission sources using modern vehicle data collection techniques, novel Lagrangian data analysis techniques, and strategies for reducing real-world emissions. The research is presented in the following chapters:

The general experimental methods are presented in Chapter 2 detailing the data acquisition, vehicle selection and mixture of routes. Each following chapter describes a study utilizing these general experimental procedures with specific alterations based on the desired setup. The order in which the chapters are presented is based upon the order of completion.

Chapter 3 focuses on energy flows consumption from conventional and series hybrid powertrain buses as well as electric and mechanical vehicle accessories through in-use testing over a wide range of climate and driving conditions. Overall the hybrid transit bus had the highest fuel economy compared to the conventional powertrain, which can be attributed to the hybrids ability for energy recapture. Half of the tests were performed using the start-stop feature on the hybrid bus, which allowed the engine to shut off at idle, however this feature had minimal impact likely due to the miss match between stop frequency and control strategy. Finally, the electrified accessories of the hybrid bus had lower energy consumption throughout all driving conditions than the mechanically driven accessories due to the direct coupling with the engine, higher frictional losses and inability

to selectively activate each accessory. The choice of route had little impact on the accessory energy consumption compared to ambient temperature.

Analogous to understanding OBD sensor and other real-world controller area network (CAN) data for the purposes of reducing vehicle emissions through next generation vehicle connectivity, Chapter 4 discusses data acquisition and analysis of a novel automatic passenger counter invention for transit applications with further significance for transit authorities. Federally-subsidized transit funding is based on ridership; therefore, it is imperative for authorities to report an accurate count of passengers. Most existing automated passenger counters (APCs) use infrared beam methods of detection. Such systems are expensive and inaccurate for some scenarios like multiple-passenger boarding or alighting. This chapter reports preliminary results from a novel APC method that has potential to improve accuracy over existing technology while decreasing overall system cost. This is accomplished through integration of existing vehicle systems including the vehicle air ride suspension (not to be confused with safety air bags), which has near universal adoption among transit buses. The system counts passengers by measuring pressure inside the vehicle air bag suspension system which directly correlates to vehicle mass. Two algorithms were developed to detect discrete boarding events based on time-resolved vehicle mass data. The first algorithm uses incremental change of vehicle mass assuming a well-calibrated average passenger mass of 168lbs (76kg) resulting in a -2.4% error. The second algorithm uses the vehicle-mass time derivative to improve the resolution of boarding and alighting events, however overall error increased to -28.4%. Experimental

testing of the mass-based APC system on an in-service transit bus showed the mass correlation method outperformed the existing infrared beam APC which had a 17.5% error, however bus kneeling events proved problematic for both the mass correlation and the event-based mass methods. Initial results are encouraging, prompting the necessity for further study and refinement. However, more work must be done to address the kneeling issue.

Chapter 5 explores in-use, spatiotemporal NO_X emissions measured from the 2013MY conventional powertrain transit bus and the series electric hybrid bus over gradients of route kinetic intensity and ambient temperature. This chapter introduces a new method for identifying NO_X emissions hotspots along a bus route using high fidelity Lagrangian vehicle data to explore spatial interactions that may influence emissions production. This work shows that the studied transit buses emit higher than regulated emissions because on-route operation does not accurately represent the range of engine operation tested according to regulatory standards. Using the Lagrangian hotspot detection, this study demonstrates that NO_X hotspots occurred at bus stops, during cold starts, on inclines and for accelerations. On the selected routes, bus stops resulted in 3.3 times the route averaged emissions factor in grams/km without significant dependence on bus type or climate. The buses also emitted 2.3 times the route averaged NO_X emissions factor at the beginning of each route due to cold selective catalytic reduction aftertreatment temperature. The Lagrangian hotspot detection technique demonstrated here could be employed in future connected vehicles empowered by advances in computational power, data storage

capability and improved sensor technology to optimize emissions as a function of spatial location.

Building upon the finding of high in-use NO_X emissions from the previous chapter, Chapter 6 compares in-use transit bus NO_X emissions from vehicles equipped with 2013 and 2015 model year (MY) conventional diesel powertrains, both certified to the same emissions standards, over a large range of vehicle operation. This study concludes that the 2015MY bus reduced tailpipe NO_X emissions by 80% compared to the 2013MY bus under real-world driving conditions. The 2013MY bus emitted NO_X at 3 to 4 times the rate of the Federal Test Procedure (FTP) certification limit during a typical transit bus route, whereas the 2015MY bus had in-use emissions below allowable limits during the FTP cycle. Improved emissions are attributed to greater NO_X conversion efficiency by the vehicle's SCR system for both low catalyst temperature and transient response scenarios as engine-out NO_X levels remained unchanged between two buses. This research proves that it is possible for SCR equipped diesel engines to meet certification cycle NO_X levels under demanding real-world driving conditions with continuous improvement to SCR dosing and thermal control strategies. Further, our results show that if 150 buses of the 2013MY from the tested fleet were retrofitted to 2015MY SCR technology, in-use NO_X emissions would be reduced by 11,000 kg per year.

Finally, Chapter 7 ventures into potential future projects including improvements the mass-based automated passenger counting system, expanded SCR retrofit studies and the future potential for connected vehicles.

Chapter 2 General Experimental Methods

Real-world studies are becoming commonplace and a preferred method of testing with the reported discrepancies between dynamometer testing and real-world use. Comprehensive instrumentation along with CAN connectivity make modern day vehicles rolling laboratories providing hundreds of simultaneous data parameters every second. More specifically, sub-systems on heavy-duty vehicles are supplied by different manufacturers, meaning that open and standardized data communication between the subsystems is necessary. This feature makes heavy-duty vehicles an ideal platform for real-world testing. The presented studies use 40' transit buses as the test platform with the following buses used as the test subjects for multiple studies. While the individual studies have slight modifications to the experimental methods, this section will describe the overarching methodology used to gather the subject data.

VEHICLE SELECTION

Two 2013 model year (MY) and one 2015MY, 2013 EPA regulation-compliant transit buses with largely different drivetrains were used for this research. The first 2013MY bus was a GILLIG 40', low-floor transit bus with a conventional Cummins ISL 8.9L diesel engine and an adaptive ZF Ecolife™ automatic transmission. The second was a New Flyer Xcelsior™ 40', low-floor transit bus powered by a Cummins ISB 6.7L diesel engine with a BAE HybriDrive™ series hybrid drivetrain and selectively enabled engine start-stop technology. The 2015MY bus was another GILLIG 40', low-floor transit bus with a conventional Cummins ISL 8.9L diesel engine, updated SCR aftertreatment system and an

adaptive ZF Ecolife™ automatic transmission. At the beginning of the study, the conventional bus had accumulated approximately 33,000 miles, the hybrid had approximately 3,000 miles, and both buses accrued roughly 18,000 miles during the testing periods. Each vehicle was equipped with a SCR aftertreatment system, oxidation catalyst, exhaust gas recirculation (EGR), and diesel particulate filter (DPF) to meet the U.S. EPA 2013 heavy-duty on-road engine certification. Furthermore, all engines were certified by the California Air Resources Board to comply with the emissions standard of 0.267 gNO_X/ kWh. All three buses have electrified EMP Cooling fans, which have been shown to reduce fuel consumption by at least 13% on transit buses [42]. Table 2.1 gives a complete overview of transit bus specifications. The buses were owned and operated by Metro Transit, the primary transit authority in the Twin-Cities, Minnesota metropolitan area.

Table 2.1: Transit bus specifications for designated test buses

	Conventional Diesel	**Series Hybrid**	**Conventional Diesel**
Model Year	2013	2013	2015
Manufacturer	GILLIG Low Floor	New Flyer Xcelsior™	GILLIG Low Floor
Engine	Cummins ISL 8.9L	Cummins ISB 6.7L	Cummins ISL 8.9L
Transmission	ZF-Ecolife™	BAE HybriDrive™	ZF-Ecolife™
Emissions	2013 Certified SCR and DPF		
AC Compressor	Thermoking Belt Driven	Thermoking 3-Phase Electric	Thermoking Belt Driven
Power Steering	Mechanical Couple	230VAC 3-Phase Electric	Mechanical Couple
Engine Fans	EMP - 28VDC Electric 8 or 9 Fan		
Air Compressor	Mechanical Couple	230VAC 3-Phase Electric	Mechanical Couple

INSTRUMENTATION

The goal of the initial study was to understand energy consumption within the vehicle along with emissions. Therefore, the collected parameters were those found to be important in identifying where energy is being consumed within the vehicle. Both light and heavy-duty vehicles are required by law to have OBD systems for the purposes of monitoring emissions control systems and ensuring emissions stay within acceptable limits [43–46]. The light-duty OBD standard is termed OBD-II, and the heavy-duty standard is termed J1939. These specify the standard protocol for intra-vehicle communication using an 8 byte data field [47]. Diagnostic trouble codes (DTCs) are messages broadcast on the CAN that alert the operator when a vehicle malfunction has occurred. Aside from DTCs, these networks broadcast many operating parameters in real time, allowing network devices to communicate with one another about their operation. These non-DTC messages were the parameters that monitored in this project. Most parameters regarding vehicle emissions and energy consumption are on the public J1939 CAN.

Further instrumentation of some accessories is required to provide a more complete understanding of vehicle operation. To monitor and process vehicle information, a National Instruments cRIO-9074 onboard controller with NI-9205, NI-9411, and NI-9853 modules was used as well as a S.E.A cRIO GXXX 3G GSM/GPS module. The data were wirelessly transmitted via file transfer protocols to the University of Minnesota Mechanical Engineering Department file server using a T-Mobile cellular carrier. Once the server received the files, a secondary computer copied those files locally, and processed them into

a MySQL server. Storage in the MySQL server allows for easy distribution of data as well as highly robust file structure and function for computation on large data sets. The files were not directly transmitted to the MySQL server to ensure data integrity due to the periodic losses in cellular communication.

TEST ROUTES SELECTION

Modern transit bus operation encompasses a wide range of operating conditions from stop-and-go traffic to 65mph hour freeway driving making it necessary to select a diverse set of routes. Kinetic intensity, the ratio of characteristic acceleration to aerodynamic velocity or square of the velocity, is a factor used to describe energy consuming route characteristics and is commonly used to define routes when comparing conventional and hybrid drivetrains [48]. Higher kinetic intensity indicates a route with frequent acceleration events and slower speeds, and conversely low kinetic intensity is indicative of higher speeds and fewer acceleration events. The test program placed the buses on three designated test routes at different times throughout the year to capture the wide range of climate, driving conditions and kinetic intensities. The three chosen Metro Transit routes (Figure 2.1) are: Route 21, an inner city route with frequent stops, high kinetic intensity (KI = 2.45 ± 0.11 km^{-1}), and relatively slow average speed (17 kph average) where opportunities for regenerative braking are frequent; Route 46, a medium speed route (25 kph average) with further distances between stops and moderate kinetic intensity (KI = 1.49 ± 0.04 km^{-1}); and route 54, an express route (28 kph average) between the MSP

Airport and downtown St. Paul with low kinetic intensity (KI = 0.61 ± 0.03 km^{-1}) resulting in few instances of regenerative braking.

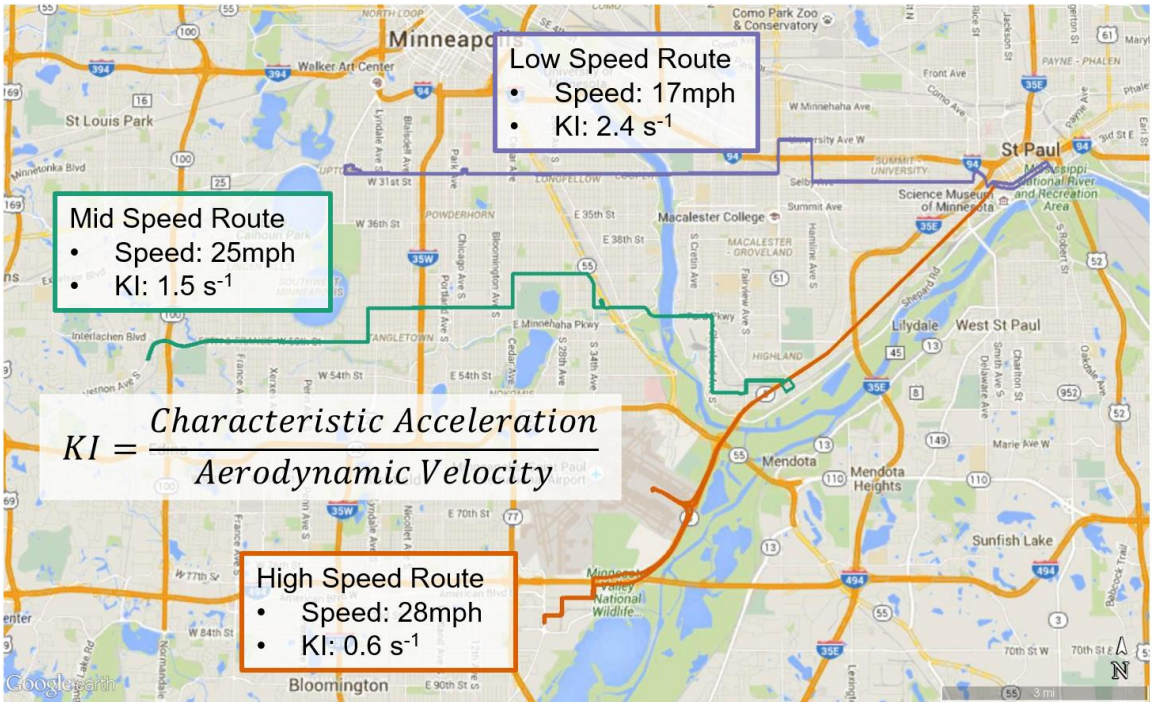

Figure 2.1: Map of selected routes along with respective statistics.

To account for climate factors, the tests were conducted during the winter season (average temperature = -14.1 ± 6.5 °C), when significant fuel was consumed to heat the bus; summer (average temperature = 21.7 ± 5.9 °C), when air conditioning was heavily used; and spring (average temperature = 13.5 ± 4.6 °C), when the climate was mild, and minimal accessory use was necessary. Furthermore, during half of each test period using the hybrid bus, the start-stop feature on the series hybrid bus, which allows for the engine to shut off when the bus is below 3 mph, was disabled to effectively provide three test buses and assess the added benefits of the start-stop feature.

Chapter 3 On-Road Evaluation of Energy Flows from New Technology Conventional and Hybrid Transit Buses

INTRODUCTION

Improving vehicle efficiency and reducing vehicle emissions is a primary focus for the automotive industry to meet emissions standards and reduce consumer fuel costs. Advances in vehicle powertrain and emissions aftertreatment have enabled drastic emission reductions from internal combustion engines allowing them continue being the prime mover of vehicles today. Specifically, mild to moderate hybridization has provided substantial fuel economy improvements due to the ability to recapture energy through regenerative braking or use of plug-in grid power [49–53].

While the majority of power consumption is used to propel the vehicle, a portion of this energy is used for auxiliary loads such as air-conditioning, heating, power steering and engine cooling, with vehicle air conditioning being the largest hotel load [54,55]. Studies suggest that complete accessory electrification could reduce fuel consumption [56] with estimates up to 15% [42], thus improving the efficiency of these components and reducing emissions. A study by Redfield et al. looked at using a hydrogen fuel cell auxiliary power unit (APU) to power vehicle accessories including the engine cooling, water pumps, air conditioning and air compressor. The findings indicate a nearly 98% reduction in accessory fuel consumption based on assumed engine, fuel cell efficiencies and cross-country trip drive cycle, however the comparison to mechanical components was based on calculated values and not actually tested in this study [56]. Another study by Campbell et al. examined

accessory power consumption from mechanically driven accessories based on in-direct sensor measurement and manufacture provided power consumption data [42]. Estimations of fuel savings from electrification were made based on accessory power consumption during times when the accessory was not in use (ie. frictional loses from a disengaged, spinning compressor wheel), but no actual comparison to electrified accessories was performed.

This study compares two modern technology transit buses to understand the real-world impact of hybridization and accessory electrification. One bus had mechanical accessories and the other had electrified accessories. Both buses are compared side by side over a wide range of route and climate conditions to provide a broad understanding of the efficiency gains from hybridization and accessory electrification.

EXPERIMENTAL METHODS

Test Vehicle Selection: The two 2013MY, 2013 EPA regulation-compliant transit buses were used for data presented in this chapter. The first bus was equipped with a conventional diesel engine and the second had a series hybrid drivetrain. At the beginning of the study the conventional bus had approximately 33,000 miles on it, the hybrid had approximately 3,000 miles, and both buses accrued roughly 18,000 miles during the testing periods.

Test Route Selection: The slow, medium and fast routes as described in Chapter 2 were used in this study. To account for climate factors, the tests were conducted during the winter season (average temperature = -14.1 ± 6.5 °C), when significant fuel was consumed to heat the bus; summer (average temperature = 21.7 ± 5.9 °C), when air conditioning was

heavily used; and spring (average temperature = 13.5 ± 4.6 °C), when the climate was mild, and minimal accessory use was necessary. Furthermore, during half of each test period, the start-stop feature on the series hybrid bus, which allows for the engine to shut off when the bus is below 3 mph, was disabled to effectively provide three test buses and assess the added benefits of the start-stop feature.

Instruments: Fuel consumption and electric accessory power consumption was measured by accessing vehicle data through the SAE J1939 heavy-duty CAN and National Instruments controller as described in Chapter 2.

Data Analysis:

Route Average Calculation – To understand the accessory contributions it was necessary to separate unique passes throughout the day by using spatial algorithms to isolate end-of-route regions from the global positioning system (GPS) information with a new pass being defined as the data from the event series of a bus entering an end-of-route region, exiting the region and immediately prior to reentering the next region. Next, the average fuel consumption in miles per gallon (MPG) and accessory power consumption in kilowatts of the air conditioning, power steering and air compressor for each pass were taken to generate a data point per pass. With accessory use being heavily dependent on ambient temperature and fuel consumption being dependent on route statistics, Figure 3.1 binned passes based on season and route. To further identify the dependence of accessory power consumption on temperature, Figure 3.2 shows binned individual power

consumption in 10°F increments. The average of each specified bin was determined along with the 95th percentile to generate the final data point and error bars.

Electric Accessory Calculation – For the series hybrid bus, the electric accessories are powered with 230VAC from the hybrid bus auxiliary power unit or APU. This 230VAC line solely powers the air conditioning, power steering and vehicle air compressor, and the combined power consumption of all accessories on this line are broadcast the J1939 CAN network. To separate these values it was necessary to generate "signatures" or known power consumption patterns indicative of each accessory. First, the air conditioning power consumption was separated using the additional data parameter of AC compressor suction and discharge pressure. When the pressure difference between the suction and discharge pressures was greater than 165 kPa, 3.5 kW was subtracted from the 230VAC power consumption statistic based on the average power consumption provided by the manufacture. The remaining power from the 230VAC line was that of the power steering and air compressor. A low-pass filter was used to further separate the power steering and air compressor power consumptions with short transient signals being indicative of power spikes from turning and long sustained power consumption being that of the vehicle air compressor.

Mechanical Accessory Calculation – All power consumption values from the mechanical accessories were made using indirect measurements and data provided by the manufacturers. For the air conditioning system, power consumption was dependent on a ratio of the engine speed as broadcast by the vehicle CAN network and AC compressor

loading. The compressor has three loading stages including unloaded, half and full load, which were measured using analog signal inputs to determine the level of loading. The air compressor power was determined by using the drive ratio of the engine speed as broadcast by the vehicle CAN network and two additional analog sensors measuring the air tank and ambient pressure. As the air tank pressure increased, the power required to compress the air increased. Finally, the power steering power consumption was determined by using a manufacturer provided map based on engine speed and pump outlet pressure.

RESULTS AND DISCUSSION

Ambient temperature during the study ranged from -17°F to 90°F, providing a wide range of climates and operating conditions. Over 1200 uniquely identified passes of the route were recorded throughout 66 total days of testing generating nearly 13 gigabytes of vehicle data. The series hybrid bus data were separated into days with the engine start-stop feature active denoted as Series Hyb. SS and days with the feature turned off denoted as Series Hybrid. Figure 3.1 shows route average fuel economy and accessory power consumption broken up by bus, climate, and route.

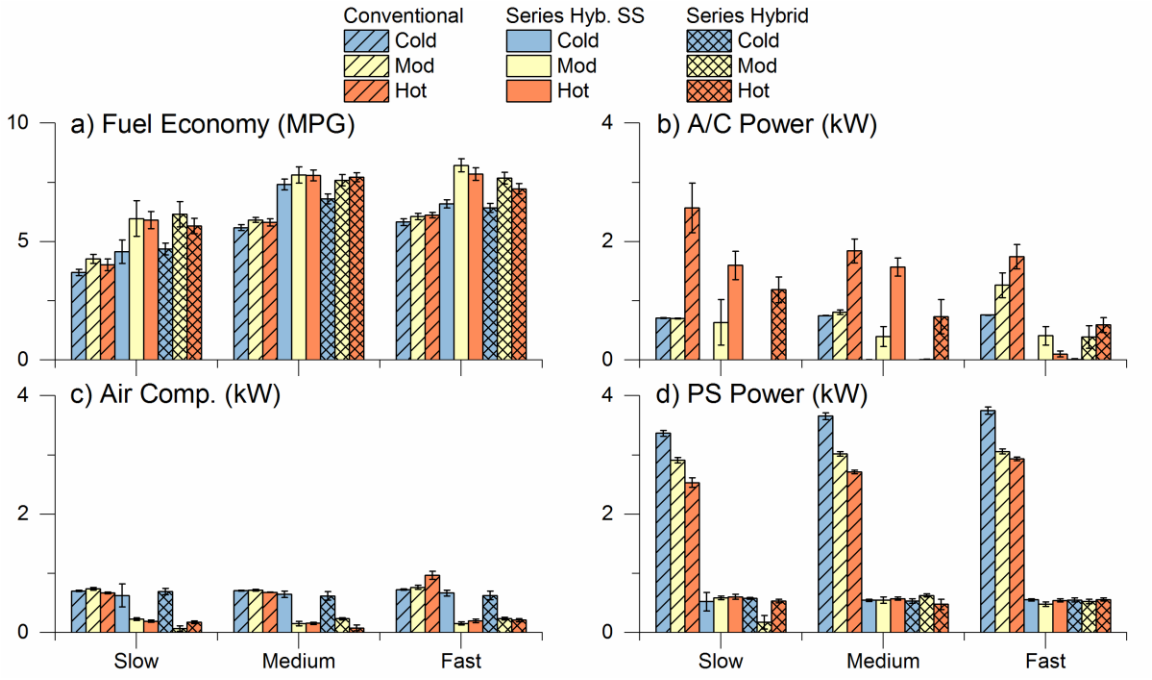

Figure 3.1: Route average comparison of a) Vehicle fuel economy in MPG; b) Air conditioning power consumption in kilowatts; c) Air compressor power consumption in kilowatts; and d) Power steering power consumption in kilowatts broken up by route and test period.

Figure 3.1.a provides the cycle average fuel economy for each route and season showing higher overall fuel economy for the series hybrid bus. Overall, the start-stop feature of the series hybrid had little effect on vehicle fuel economy, however there was a statistical improvement on the high-speed route, which is counterintuitive since there are fewer opportunities to recapture energy. Slower routes generally have more stops which intuition dictates would provide more opportunities for saving fuel using the start-stop feature, yet there was little difference on the slow route. This finding is likely attributed to the effectiveness of the stops on each route. Cummins specifies that after the engine is shut

off for start-stop operation it must run for two minutes before another shutdown is allowed. This physically limits the engine to 30 start-stops per hour. Therefore, if the engine shuts-down prematurely in stop-and-go traffic, it might only shut off for an instant and remain on for the following 2 minutes at idle. Conversely, the high speed express route has long distances between stops and longer layovers providing ample time before each stop and longer braking distances.

The remaining plots in Figure 3.1 provide the cycle average accessory power consumption for each route and season showing that route type had little impact on accessory power consumption, and the largest factor influencing accessory power consumption was temperature. To examine ambient temperature dependence, Figure 3.2 shows route average accessory power consumption plotted against average temperature for both mechanical and electrified accessories.

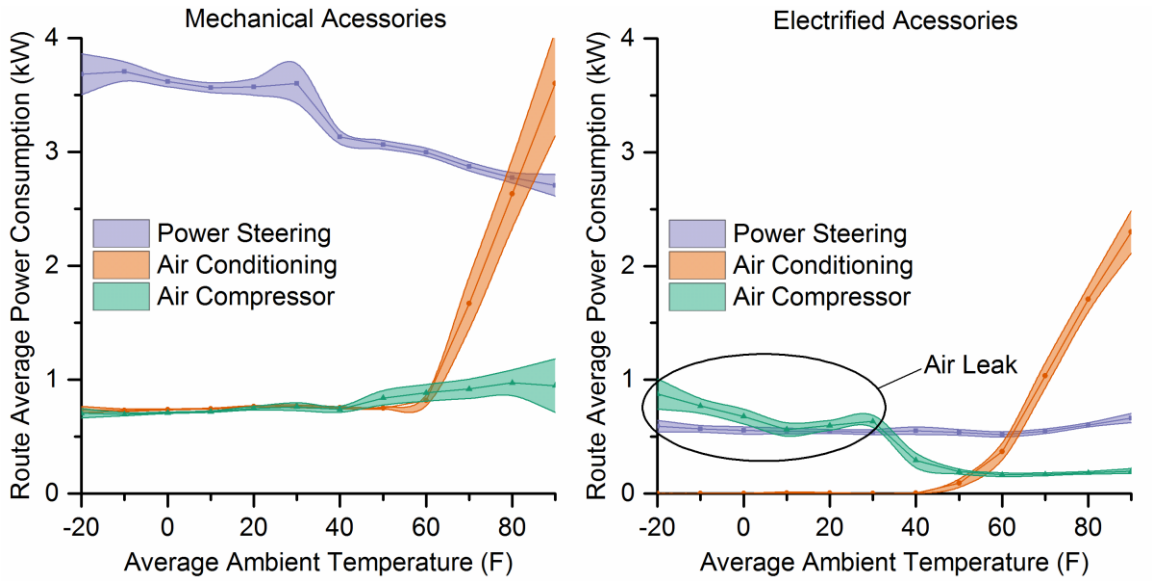

Figure 3.2: Accessory power consumption versus average ambient temperature.

Air Conditioning: Depending on ambient temperature, the electrically driven AC unit used between 35.1% and 100.0% or 0.4kW and 1.3kW less power than the mechanically driven unit, which had a constant power load of approximately 0.75kW at the lower temperatures when the AC is turned off. This can be explained by frictional losses from the constant spinning of the unloaded compressor.

Power Steering: The electrically driven power steering consumed between 75.5% and 85.0% or 2.0kW and 3.1kW less power than the mechanically driven system, which can be attributed to the mechanical system's direct gear coupling to the engine and inability to unload when not in use. The mechanically driven system also exhibited a steady downward slope. The steady downward trend is likely a result of decreasing fluid viscosity with increasing temperatures.

Air Compressor: Data derived from the vehicle air compressor accessory, which is used to supply air to the vehicle's air suspension and brakes, showed similar trends as the other accessories with the electrically driven compressor having between 60.5% and 81.7% or 0.4kW and 0.8kW less power consumption than the mechanically driven counterpart. However, an identified air system leak substantially increased power consumption values for the electric compressor at temperatures lower than 40°F compared to those in the summer months. Likely if this test were repeated with the air leak fixed, the power consumption values would be similar throughout all temperature ranges.

CONCLUSION

This work evaluated fuel economy and energy flows from conventional and series hybrid powertrain vehicles through in-use testing over a wide range of climate and driving conditions. Overall the hybrid transit bus had the highest fuel economy compared to the conventional powertrain, which can be attributed to the hybrids ability to recapture and reuse energy. Half of the tests were performed using the start-stop feature on the hybrid bus, which allowed the engine to shut off at idle. However, this feature had minimal impact likely due to the miss match between stop frequency and control strategy. Overall, the electrically driven accessories had between 56.5% and 82.4% or 3.6kW and 4.1kW less power consumption throughout all driving conditions due to the indirect coupling with the engine, lower frictional losses and ability to selectively activate each accessory. The choice of route had little impact on accessory power consumption. Ambient temperature had the largest impact on accessory power consumption with the air conditioning power consumption having a direct correlation to temperature and the power steering power consumption having an inverse correlation to temperature due to increasing viscosity of the working fluid.

Chapter 4 Mass-Based Automated Passenger Counter: An Application for Future Vehicle Data Collection and Analysis

Modern day on-road vehicles come standard with CAN, enabling OBD access to real-time vehicle performance and operational data. Further, this information can be collected using a low-cost microcontroller making vehicle testing and data recording readily accessible. This chapter discusses the development of a novel mass-based automatic passenger counter to provide a more accurate, lower-cost passenger counting method which can be retrofit on existing transit buses. This study illustrates the process behind vehicle data collection for developing the algorithms to count passengers using bus mass, and offers a use-case for future vehicle connectivity.

INTRODUCTION

Automatic passenger counters provide passenger boarding/alighting information associated with time and location data. APCs are a standard tool used by transit authorities to measure and report monthly ridership to the National Transportation Database (NTD) with resulting federal subsidies calculated solely based on the data they provide [57]. Additionally, these data provide vital insight into passenger behavior and perception of bus service for purposes of service development [58–60].The most accurate APCs currently count 98% of passengers and cost approximately $8,000 per unit (each bus would have at least one unit per door) with cost proportional to accuracy [61,62]. Buses provide the largest fraction of public transport servicing over 52% passenger trips in the U.S. [63], and as of 2008 over 840,000 buses were registered nationwide [19]. With 80% of transit agencies using APC

systems [58] and smaller authorities disproportionately using manual counts due to budgetary constraints, a need exists to improve the accuracy of current systems and lower costs. This can be done through systems that integrate with existing hardware and software available on buses such as automatic vehicle location, GPS and CAN systems that continuously broadcast vehicle and powertrain data.

Commercially available APC systems can be categorized by detection method. Sensors include infrared (IR) light beam cells, passive infrared detectors, video cameras, infrared cameras, laser scanners, ultrasonic detectors, microwave radars, piezoelectric mats and switching mats [64]. Sources of inaccuracy common among all systems include improper calibration, vehicular assignment when only a few APC systems are available and the ability to analyze the volume of collected data [65].

The most common APC technology used by transit agencies, and the one used for comparison in this paper is the IR beam break or light barrier method [58]. This system uses multiple infrared beams crossing the door well at the front and back of the bus providing direction and count of passengers boarding and alighting. Directionality of the passenger's movement is determined from the sequence in which the beams are broken [62]. A passenger entering will break the beam closest to the door first, and a passenger leaving will break the beam furthest from the door first. Passenger count is stored on-board the bus until it returns to the garage where the day's data is uploaded to a database. This information is stored for multiple years and is easily accessible. Though light barrier APCs can be over 95% accurate [66], miscounts are known to occur when multiple people board through the

same door simultaneously or from passengers boarding in close proximity to one another. IR-based APCs are also known to overestimate passenger loads by a statistically significant margin [65] irrespective of bus type, thus an internal correction factor is generally used for passenger load estimates.

More novel APC methods include those described by Greneker, et al. [67] who developed a unique pressure mat APC device consisting of a thin pressure sensor mat located on the floor near the boarding door and fare box, a microprocessor for evaluating electronic images produced from the pressure patterns of a passenger's shoe resting on the mat, and algorithms to translate mat data into people counts. Sources of error were found to be caused by biased mass including passengers carrying small children, packages, bicycles or other objects aboard the transit vehicle that interfered with the mass data collected by the mat. The system was reported to be approximately 87 % accurate [68].

Bauer, et al. [68] evaluated performance of the two comparatively inexpensive sensing technologies, light barrier and switching mat for passenger count and measurement of service times at the Vienna airport, security and border checkpoints. The security checkpoint setting was seen to be a harder test case since a significant number of passengers were required to repeat the security procedure, resulting in bidirectional traffic not differentiated by the sensors. Results showed that both sensing technologies were able to obtain accurate counting for an aggregation of several hours, but flow counts for shorter time periods (5 to 15 min) were less reliable. The switching mat outperformed the light barrier sensor in the border setting and performed slightly worse in the security checkpoint

setting, where the placement of the mat was not optimal. Consequently, in terms of counting passengers, the switching mat was the better system.

Peterson [69] evaluated the technical, operational, and economic feasibility of using medium-range radio frequency identification (RFID) technology to track transit passengers on the North Dakota State University (NDSU) Transit System. The RFID tags used at NDSU were attached to the outside of student backpacks allowing for little interference between the card and the reader. Controlled tests indicated that the reader received a valid signal from the RFID card if it was in plain sight and there was no interference present. When riders boarded the bus with the card either in their pockets or against their cell phones, the read quality dropped dramatically [69]. A card's ability to read is highly dependent on the visibility to the receiver device [70]. The analysis showed that with proper ridership numbers and varying percentages of non-student riders, RFID technology can provide an economic benefit to transit agencies. Improvements in sensor technology would improve performance. However the requirement of all riders to have a card to be counted could affect accuracy [69].

This study presents a preliminary evaluation of a novel APC technology which aims to improve upon existing methods by using vehicle mass to assess boarding and alightings of passengers on transit buses. Unlike the pressure mat method that only measures mass at the door locations, our system measures the change in mass of the entire cabin derived from three pressure sensors mounted in the vehicle suspension system. Vehicle passenger load is directly proportional to vehicle mass, therefore chances for miscounts can be

reduced. With increased integration of existing vehicle information systems, the mass-based APC system has potential for lower cost and could provide additional information of interest to transit authorities like route-specific passenger distribution within the bus or passenger load contributions to fuel consumption.

METHODS AND EXPERIMENTAL DESIGN

Air Suspension Systems: Development of air ride suspension began in the late 19th century with use on vehicles beginning in transit buses. Today, trains, buses, tractor trailers, and even passenger cars use air ride suspension with near universal adoption on mass transit as well as trucks and trailers [71]. Modern transit buses are factory equipped with air ride suspension to provide a smooth ride to passengers while maintaining vehicle ride height. Air ride prevents bottoming out during large load changes experienced from passengers boarding or alighting the bus. A mechanical auto-leveling valve maintains the ride height by increasing or decreasing the air pressuring inside the bag when an increase or decrease in cabin load is experienced. In other words, as passengers board the bus, pressure increases within the air suspension; alighting produces the opposite result.

The entire suspension system consists of three air circuits with two connected air bags on each circuit for a typical forty-foot transit bus like the one used in this study. Figure 4.1 shows the location and connections of each air circuit. Connections between air bags indicate that air pressure is equal in connected bags. Common nomenclature when referring to sides of a bus includes “curb side”, which is the right side or passenger pickup side

adjacent to the curb, and “street side”, which is the driver’s side of the vehicle. Standard forty-foot buses have curb side, street side, and front air bag circuits.

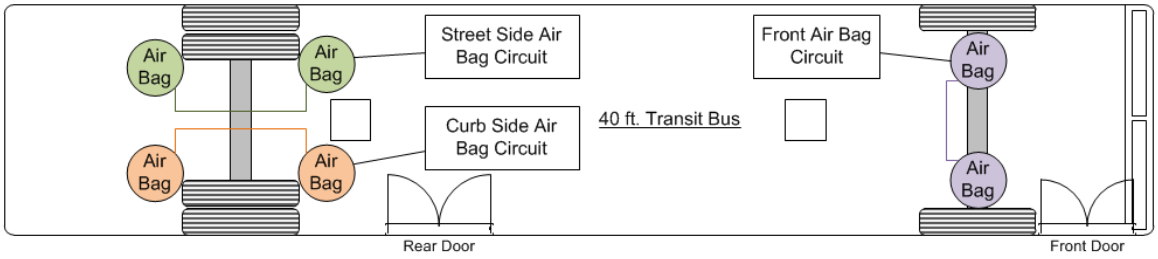

Figure 4.1: Plan view of a 40 ft. transit bus indicating the air bag suspension system. Three air bag systems control the street side rear axle, curbside rear axle, and front axle.

Using knowledge of the correlation of air suspension pressure with vehicle load and the connection between the paired air bags, pressure transducers are placed on each air bag circuit to monitor vehicle mass in real time. Calculation of the bus mass m_{bus} is done using Equations 4.1 and 4.2 below. Equation 4.1 gives the measured mass of the bus where m_m is the measured mass, *a*, *b*, and *c* are the effective air bag surface areas of the front, curb, and street side air bags respectively, and P_{Front}, P_{Curb}, and P_{Street} is the pressure measured in each respective airbag. Equation 2 relates the measured mass of the bus to its actual mass accounting for pressure induced from the air bag’s elastic rubber membrane. The constant *b* is the proportion between know mass change and measured mass change, similarly *K* is the constant difference between the know mass and the actual mass. The values of the constants A_{Front}, A_{Curb}, A_{Street}, *b*, and *K* are found using a calibration procedure described in the calibration and validation section.

$$m_m = A_{Front} * P_{Front} + A_{Curb} * P_{Curb} + A_{Street} * P_{Street} \quad 4.1$$

$$m_{bus} = b * m_m + K \quad 4.2$$

Knowing the contribution to overall bus mass from three locations, it is also possible to determine general passenger location within the bus. Further, since the airbag system is independent of activity at the doors of the vehicle, the bidirectional and multiple boarding events are distinguishable when mass is known as a function of time.

Raw Data Filtering and Processing: This section presents the method of filtering and processing the raw mass data gathered from the system. Each of the three pressure transducer signals are processed through a Savitzky-Golay smoothing lowpass filter using a local least squared polynomial approximation [72] to reduce signal noise. Figure 4.2 shows an example of the filtered versus unfiltered pressure transducer data. Reducing signal noise helps improve the quality of the inputs to the mass calculation. The three filtered pressure transducer signals are then used as inputs to Equations 4.1 and 4.2 which produce instantaneous vehicle mass. A byproduct of calculating mass from three separate signals is a small high frequency fluctuation in the mass output inconsistent with passengers boarding. This mass calculation artifact was mitigated using a low pass filter with a lower cutoff frequency of 1 Hz derived from the approximate boarding event duration of 1 second.

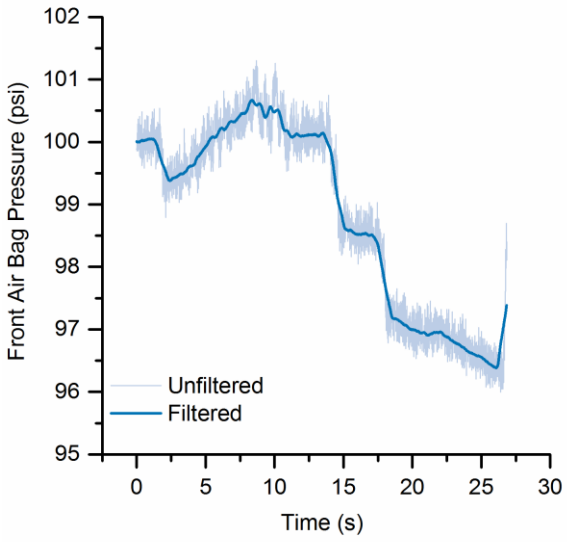

Figure 4.2: Example of filtered versus unfiltered front airbag pressure versus time as measured on a transit bus.

Passenger Counting Algorithms: Based on the raw air bag pressure measurement, two algorithms were developed to calculate passenger count. The first uses additional mass and an assumed average passenger weight and the second is an event-based method determined from the time derivative of mass.

Additional Mass Method – The first method for determining passenger count is the additional mass method, which correlates additional vehicle mass with passenger count. In this method a standard passenger mass m_p of 168lbs (76 kg) was chosen in this study. After each stop, the current passenger count L_C is calculated using Equation 4.3 below where m_{bus} is the total bus mass and m_{curb} is the curb mass of the bus.

$$L_C = Round\left(\frac{m_{bus}-m_{curb}}{m_p}\right) \quad 4.3$$

Event-Based Method – The next method for examining passenger count was to look at the individual passenger loading events. 100Hz Data is required for this method to give a high-resolution view of mass change events not possible with the stop aggregated data used in the previous method. The key to counting mass change events is to study the time derivative of the mass trace. When the derivative passes a threshold of +75lbs per second (34 kg/s) a boarding is counted. Similarly, when the derivative goes below a threshold of -75lbs per second (-34 kg/s) an alighting is counted. Current passenger load is produced from the sum of the previous passenger load, boardings, and alightings. Figure 4.3 illustrates the logic used to determine these counts, and Figure 4.4 exemplifies and optimal scenario for detection of a boarding event.

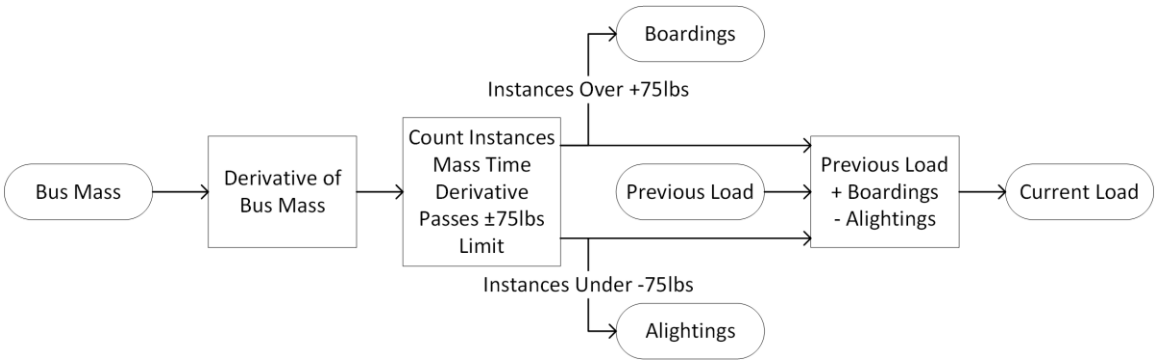

Figure 4.3: Diagram of mass change event logic.

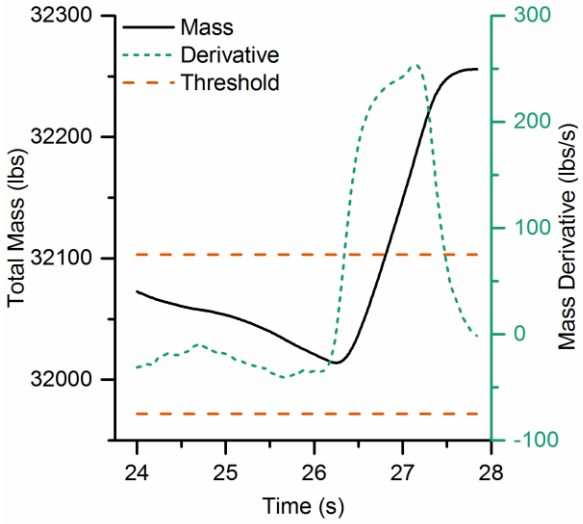

Figure 4.4: Example of mass and derivative during mass change event.

Data Collection and Experimental Design: The transit bus used in the study was a Low Floor GILLIG forty foot bus operated by Twin Cities Metro Transit, Minneapolis, MN. It was equipped with a Neway 4-bag rear suspension and a GILLIG Air Ride front suspension system. Pressure from each air bag circuit was measured using the onboard National Instruments C-RIO microcontroller programed to collect pressure sensor data at a 100Hz rate as well as 1Hz aggregated data. To reduce processor load 100Hz data were only collected at vehicle speeds less than 3 mph (4.8 kph) as determined by the CAN signal. 100Hz data collected at speeds over 3 mph (4.8 kph) produced inaccurate weight measurements resulting from vertical movements of the bus reacting to the road surface. Pressure data combined with CAN and GPS data, was stored locally and sent using a cellular card for real time remote processing. Wireless transmission eliminates the requirement for transit agencies to manually download APC data, which is a desirable

quality of these systems [58]. Figure 4.5 illustrates how data is collected, processed and stored in the mass-based APC system. To compare with existing APC technology, time and location stamped passenger count and passenger miles traveled were produced with our system along with the passenger mass and distribution of mass within the bus.

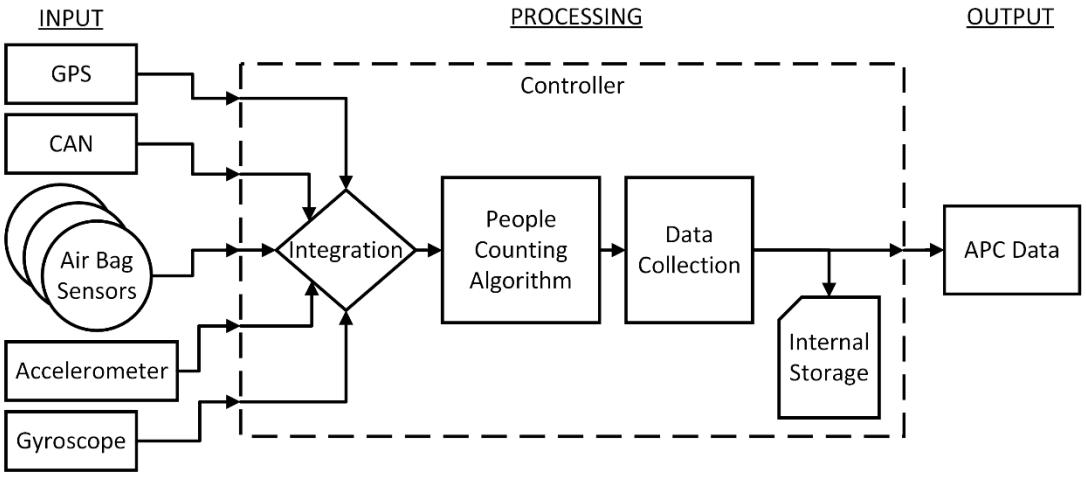

Figure 4.5: Signal flow diagram of mass-based APC design.

Calibration and Validation: To determine coefficients for mass Equations 4.1 and 4.2, a static calibration procedure was performed involving loading the bus with known mass to measure the corresponding airbag pressures. Pressure measurements with the bus unloaded were taken first followed by increasing mass in 250lb (113 kg) increments up to 1000lbs (454 kg) using stacks of 50lb (23 kg) sand bags. This process was repeated over the front, street side, and curb side airbag circuits to provide the largest variability in mass distribution and enough measurements to solve for A_{Front}, A_{Curb} *and* A_{Street} in Equation 4.1 using inverse matrix multiplication. Setting known bus curb weight as the unloaded mass, coefficients *b* and *K* were found using the calibration data as input into Equation 4.2. After

calibrating the bus, a test run was made around the block with one boarding and alighting event to make sure everything was working properly. The calibration process for this device is similar to the IR beam sensors where manual counts are required for determining boarding and alighting correction factors [65].

During the experimental study, IR beam APC data along with security video footage were used to validate passenger counts. The IR light beam APC factory installed in the tested bus is a Trapeze Transit Master Automatic Passenger Counter which has a reported 95% accuracy according to the manufacturer [66]. Manual counts from video footage provided the known passenger count used to assess APC accuracy. Video cameras are installed in all buses in Metro Transit's fleet which watch the doors and cabin as well as provide a view out the front window. Unlike the APC data, video footage is only kept for 30 days and only viewed in the event of an accident or when security incidents occur on the bus.

Experimental results presented here were taken from a single bus operating during one day of service. Mass based APC data, IR beam APC data, and video data were recorded. Metro Transit route 675 was the designated test route with service between Minneapolis and Mound, MN. This route was chosen for its wide range of driving conditions to cover the different types of settings a transit bus encounters. Features of the route include slow city driving with frequent stops, high speed highway sections, and suburban service with long distances between stops.

RESULTS AND DISCUSSION

Static Mass Calibration: The results of the static calibration procedure are shown in Figure 4.6. The resulting trendline equation is the calibrated form of Equation 4.2 where y is m_{bus} and x is m_m, and the coefficients 0.9277 and 14,508 are b and K respectively. Figure 4.6 indicates that measured mass from airbag pressure has a linear relationship with actual loading which is expected.

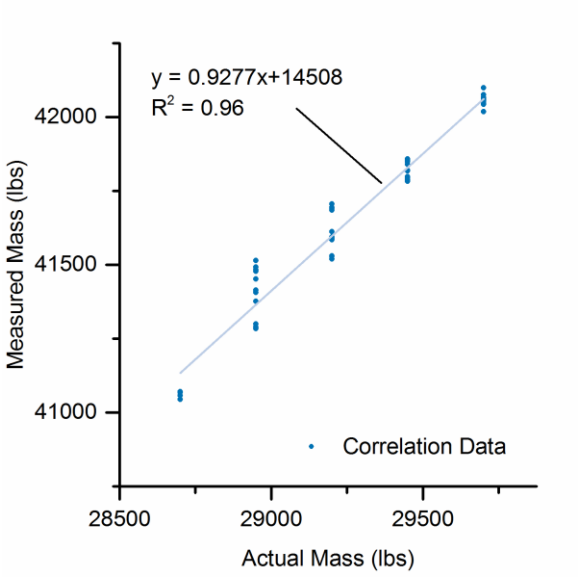

Figure 4.6: Mass calibration results showing measured bus mass versus known bus mass.

On-Route Passenger Counting: Figure 4.7 shows the comparison between additional vehicle mass over the curb weight and manual passenger count for the on-route testing. Each data point in the figure represents an individual bus stop event. Vehicle mass and passenger count are linearly correlated. Excluded data shown in the figure are erroneous points resulting from the bus deflating its front airbags to kneel the bus. In these kneeling

events, the air bag pressure was no longer an accurate measure of total vehicle mass from the resulting negative excess-mass values. However, the rear airbag suspension circuits were still active during kneeling events providing some resolution of happenings within the bus. One of the key benefits to an air bag suspension is the kneeling feature for ease of access, so resolving this issue will be a focus of further research. Eliminating data from kneeling events gave a higher residual value for the linear fit line. Average passenger mass, given by the slope of the line, also increased. The calculated average passenger mass was 168 lb (76 kg), a believable estimate for an average adult based upon national data [73].

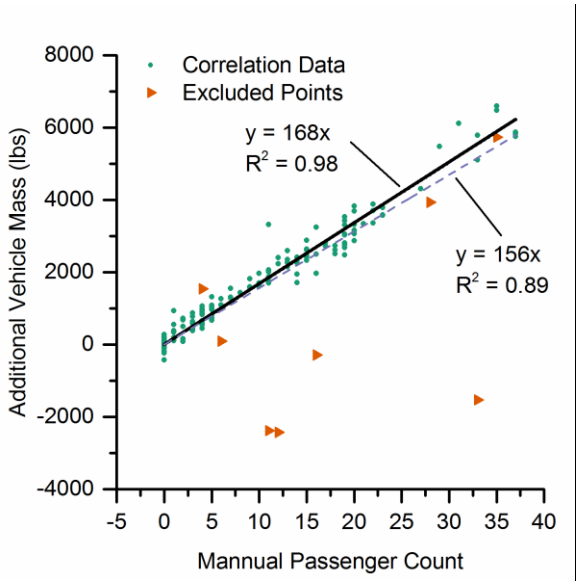

Figure 4.7: Graph of additional vehicle load versus passenger count.

The event-based method was applied to compensate for the additional mass algorithm's inability to measure passengers during kneeling events. Discrete boarding and alighting events were counted when the derivative of the vehicle mass crossed a threshold of plus or minus 75 lbs per second (34 kg/s). The results of both methods along with the video count and IR beam APC count are shown as cumulative trip passenger count in Figure 4.8. Both

the IR beam and event-based APC counts were artificially set to zero at the end of each pass of the bus route so error wouldn't compound from one pass to the next.

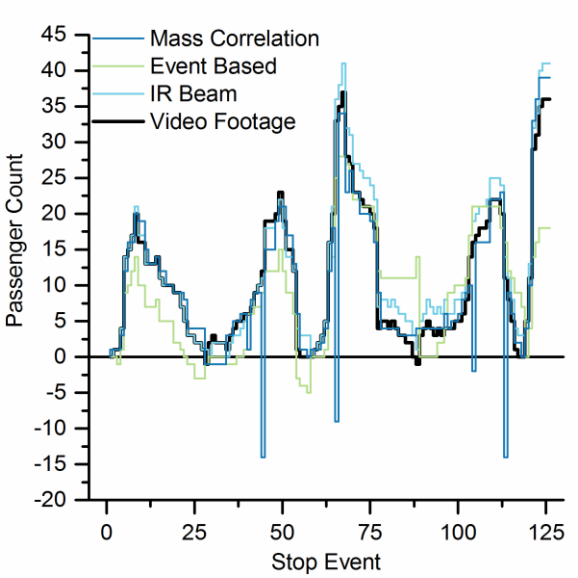

Figure 4.8: Comparison of the three different passenger count datasets including the two mass based methods.

The factory-installed IR beam APC followed passenger count patterns accurately but the total count per route pass was consistently overestimated. The IR beam APC passenger count was unaffected by the kneeling of the bus since it does not depend on the pressure in the air bags. However, the IR beam APC has some error. Situations like people standing in the rear doorway, when the seats are full, or passengers bringing bikes and personal belongings aboard caused the IR beam APC to over-count the number of passengers. Passenger count based solely on additional bus mass closely matched actual count established form the video footage; however, if the average passenger mass deviated significantly from 168lbs (76 kg), miscounts resulted. Also, passenger count was heavily

affected by the kneeling of the bus. The event-based mass APC algorithm consistently underreported passenger number. However, it did improve passenger count during kneeling events compared to the additional mass-based APC method.

Using the equation from Kuutti [64], Table 4.1 shows the error of the three APC methods studied compared to the manual count for the entire test period. The additional mass APC method was the most accurate method followed by the IR-based method. The event-based mass APC was least accurate of the three methods resulting from multiple stops where closely spaced boardings occurred. Instances where several passengers boarded in rapid succession produced a single derivative peak causing the event-based APC to count many boardings as one.

Table 4.1: Error Comparison between APC Methods

	Manual Count	*IR beam APC*	*Event Based Mass APC*	*Additional Mass APC*
Average % Error	0.00%	17.50%	-28.23%	-2.38%

Figure 4.9 is an instance where all passenger count methods were in agreement. This figure shows total bus mass in black and its time derivative in blue for five alightings followed by one boarding event. The red lines are the thresholds the time derivative must cross to count a boarding or alighting event. From the manual video count, passengers quickly entered and exited the bus from the front giving the distinct spikes in the derivative of the mass trace.

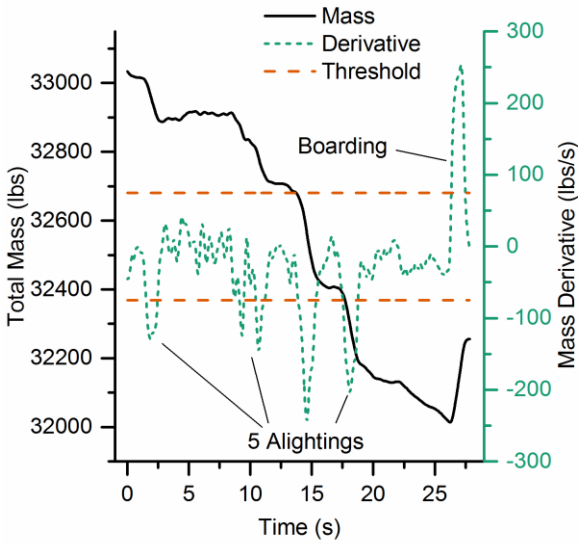

Figure 4.9: Graph of mass versus time for accurately counted stop.

There were also boarding events where the passenger count from all three APC methods was not in clear agreement. An example of this is shown in Figure 4.10. In this instance, the actual passenger count according to the video footage was three people boarding with one of those people placing a bicycle on the front bus rack. The first two boardings are clearly seen similar to the prior example, but when the third person places their bike on the rack and proceeds to board, the count becomes unclear. This third passenger also had a bag which caused a second beam break on the IR-based APC to read upon boarding. The final count from the event-based APC was 4 people boarding and 3 people alighting, the IR beam APC counted 4 boardings, and the additional mass method had a net increase of one passenger.

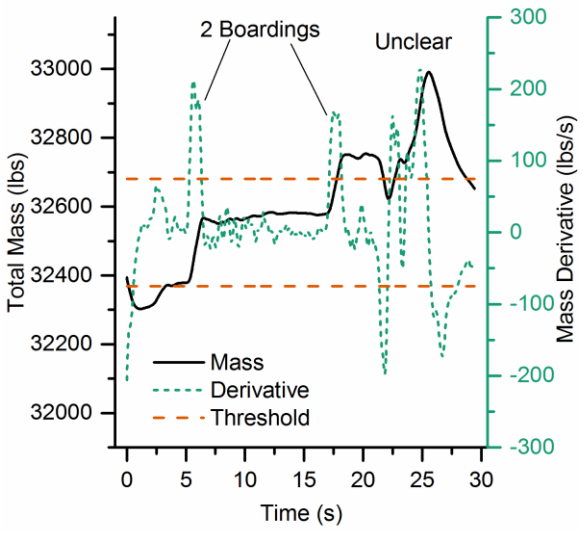

Figure 4.10: Graph of mass versus time for inaccurately counted stop.

Other events that resulted in inaccurate passenger counts included people with wheel chairs entering via the ramp causing the bus to kneel, people bringing large bags or objects such as bikes, small children playing in the entrance, people blocking the doorway sensors, and multiple consecutive boardings.

CONCLUSIONS

Using pressure data collected from bus air-ride suspension systems to measure the additional vehicle mass and thus passenger count is a novel way of providing transit agencies insight into the ridership of their buses. Results of our experimental study look promising, and our data indicate that the mass-based APC is as accurate or more accurate with the current IR beam APC technology. The mass-based APC also has the potential to provide more information than current systems such as distribution of passengers throughout the cabin. Using a properly calibrated average passenger mass, the incremental

change in mass at a stop can be synonymous with change in passenger count. To eliminate the need to know the average passenger mass, the derivative of mass can act as a measure of boardings and alightings.

Chapter 5 Lagrangian Hotspots of In-Use NO_X Emissions from Transit Buses

INTRODUCTION

Federal emissions regulations are emplace to limit harmful vehicle pollutants such as NO_X from entering the atmosphere with the intent of improving air quality.[13] Not only is NO_X a precursor to tropospheric ozone,[9,10] inhaling NO_X components and ozone causes respiratory inflammation and can worsen symptoms for those with respiratory diseases.[11,12] Therefore, locally high NO_X concentration, or "hotspots" in areas with high traffic density adversely impacts the health of at-risk populations.[74] Heavy-duty vehicle regulations described in the FTP mandated by the U.S. EPA limits the summation of power specific NO_X emissions to be 0.267 g/kWh over the standardized FTP test cycle for all on-road engines produced after 2010.[75] The use of a test cycle allows researchers and regulatory agencies to quantify and compare emissions.[76] To account for real-world influences (vocation, duty cycle, chassis integration, ambient conditions, vehicle age, maintenance and driver), an additional in-use limit or not-to-exceed (NTE) emissions limit is specified to be 1.5 times the FTP cycle limit (0.401 g/kWh).[75] This limit applies when the vehicle is within specific engine operating conditions (load, speed and coolant temperature), environmental conditions (elevation, temperature and pressure) and transmission temperature for a consecutive 30 seconds or longer.[75,77]

Recent advances in engine technology and emissions aftertreatment have allowed diesel engines to meet the increasingly restrictive emissions standards. Common NO_X reduction techniques include engine EGR which helps reduce in-cylinder NO_X formation[78]

by lowering combustion temperature and SCR aftertreatment systems to reduce tailpipe NO_X.[79] Increased stringency in emissions regulation has been shown to be the largest factor in overall NO_X emissions reduction of heavy-duty vehicles due to manufacturers incorporating theses aftertreatment devices.[80] Fully warmed SCR systems are known to reduce tailpipe NO_X emissions down to 20-30% below the regulated emissions standard indicating their high efficacy when properly implemented.

Despite stringent government regulations, studies have shown that NO_X emissions observed for in-use vehicles are far higher than mandated standards. A study by Wu et al.[20] showed that real-world NO_X emissions from Euro IV certified heavy-duty buses using SCR exhaust aftertreatment systems were substantially higher than the certified limit suggesting that the certification cycle does not accurately represent real-world conditions. Andreae et al.[81] found that poor vehicle integration and misalignment of engine certification and vehicle test cycles can be significant contributors to the emissions discrepancy. Low-load driving at slow speeds can also cause elevated NO_X emissions in heavy-duty diesel engines equipped with SCR due to low temperature inactivity of SCR catalysts.[20,24,82,83]

Where much research has explored engine-operating conditions that lead to high NO_X emissions, aligning those emissions with spatial information can indicate at-risk geographic areas. Further, identifying spatio-temporal influences on production of these emissions can provide researchers and vehicle manufacturers with a better understanding on where to focus their emissions reduction efforts and provide regulators with data for improved standards.

Spatial emissions mapping using stationary or movable ambient air monitoring stations is common practice for governments and researchers.[82,84] For example, the Minnesota Pollution Control Agency uses 53 stationary ambient air quality monitoring stations statewide to spatially determine air quality and understand emissions sources.[85] A study by Tan et al.[86] used a mobile emissions measurement platform and geographic information system (GIS) software to spatially and temporally correlate ambient air quality along road networks in Pennsylvania with 500m by 500m grid resolution. GIS software was used by others[87,88] to spatially map yearly emissions with 1 km by 1 km resolution using emissions databases containing information from multiple collection sites as well as fuel consumption inventories. Spatio-temporal datasets such as these are used to calibrate vehicle emissions and travel demand models.[74,89] Adopting a fluid flow analogy, such analyses can be viewed as Eularian; i.e., they measure emissions of passing vehicles from a stationary frame of reference to give a sense of the emissions from traffic flowing by. Figure 5.1.a provides an example of such Eularian measurements as viewed by the user. Eularian approaches do not have the spatiotemporal resolution to determine individual contributions by vehicles in traffic flow and therefore cannot be used to accurately determine acute health effects from highly localized sources of emissions from vehicles.

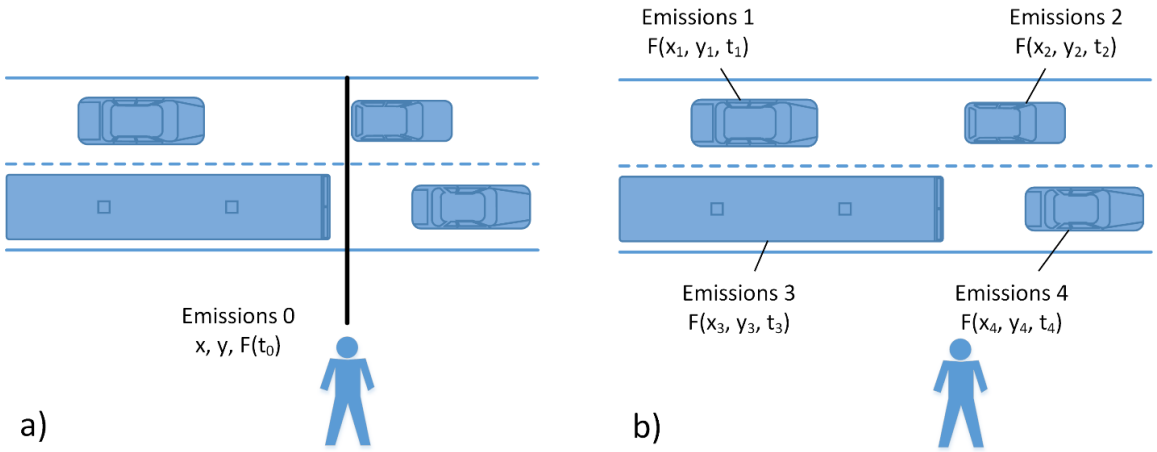

Figure 5.1: Illustration of a) traditional Eularian emissions measurement vs b) novel Lagrangian emissions measurement.

Conversely, Lagrangian data taken from the vehicle frame of reference can more precisely indicate the spatio-temporal distribution of mobile emissions sources. An example of Lagrangian emissions measurement where readings are taken from the vehicle frame of reference is shown in Figure 5.1.b. Typically, emissions source modeling is used to estimate individual vehicle contributions to emissions by using emissions factors in g/km for different ranges of vehicle speed. For example, specific to transit buses, Gouge et al.[74] used emissions modeling with GPS data collected from buses to estimate NO_X in 50m intervals enabling them to identify emissions hotspots along a transit route which showed that intervals near stops and major intersections resulted in emissions 1.6 to 3.0 times the average. However, these findings were not substantiated with experimental emissions data and the study did not take into account operational effects on emissions production rates. Little previous work has examined Lagrangian NOx hotspots from in-use data. In another study, Unal et al.[90] used portable emissions monitoring systems onboard transit buses to

identify emissions hotspots along a specified route finding that signalized intersections can contribute to increased emissions. While containing the key underpinnings to spatial emissions hotspot analysis, the study was very limited in scope examining only 23 lengths along the bus route. Further, GPS devices were not used, making location tracking tedious and unusable for applications of larger scope.

This work shows how Lagrangian spatial emissions mapping techniques using data recorded from manufacturer-installed tailpipe NO_X sensors in two transit buses can identify systematic and physical causes for elevated in-use emissions from hybrid and conventional powertrain transit buses over a gradient of route and ambient temperature. Performed on a large dataset collected over three seasons, this demonstrates spatial influences on vehicle emissions and develops a method for spatial vehicle emissions analysis that could be applied to larger datasets.

EXPERIMENTAL METHODS

Test Vehicle Selection: The two 2013 model year (MY), 2010 EPA regulation-compliant transit buses were used for data presented in this chapter. The first bus was the conventional diesel engine and the second was the series hybrid drivetrain. At the beginning of the study the conventional bus had approximately 33,000 miles on it, the hybrid had approximately 3,000 miles, and both buses accrued roughly 18,000 miles during the testing periods.

Test Route Selection: The slow, medium and fast routes as described in Chapter 2 were used in this study. To account for climate factors, the tests were conducted during the

winter season (average temperature = -14.1 ± 6.5 °C), when significant fuel was consumed to heat the bus; summer (average temperature = 21.7 ± 5.9 °C), when air conditioning was heavily used; and spring (average temperature = 13.5 ± 4.6 °C), when the climate was mild, and minimal accessory use was necessary. Furthermore, during half of each test period, the start-stop feature on the series hybrid bus, which allows for the engine to shut off when the bus is below 3 mph, was disabled to effectively provide three test buses and assess the added benefits of the start-stop feature.

Instruments: NO_X emissions were measured by accessing data from sensors associated with the SCR system through the SAE J1939 heavy-duty CAN and National Instruments controller. These sensors are necessary for proper exhaust aftertreatment operation whereby engine outlet NO_X and tailpipe NO_X measurements direct the system's urea injection for the catalytic reduction process and signal the vehicle operator if faults occur. The onboard NO_X sensors have an accuracy of ±10ppm from 0 to 100ppm and ±10% from 100ppm to 2000ppm.[91] Data where the sensors are turned off or warming up was removed to ensure erroneous data is not incorporated into results.

Data Analysis

FTP Comparison – Traditionally, test cycle comparison to in-use data is performed using binning methodologies[76] where a given vehicle speed trajectory is broken into kinematic sequences with each subsection given a probability of occurrence based on various metrics including duration, distance, velocity, acceleration and drive type. However, this methodology breaks down when analyzing heavy duty test cycles due to the

large number of possible operating conditions produced by the simultaneous engine torque and speed trajectories. To properly compare in-use data to heavy duty test cycles a multi-dimension normalized cross correlation similarity measure was used as described in a study by Penney et al.[92] which compared accuracies of different similarity measures when used to associate medical scans consisting of two different intensities images. While new to the engine and emissions field, such analyses are commonplace in the medical and data science communities. Translating this methodology for purposes of test cycle comparisons the percent engine speed versus torque axis equate to the X and Y image pixel locations, and the percentage of time spent at each engine operating point equates to pixel intensity. This measure was chosen because of its dependence on pixel or operating point intensity. If the engine spends a majority of its time at a single point, that point will be more heavily weighted. First the engine operating profiles were normalized for both the FTP cycle and collected in-use data in terms of percentage of max operation according the FTP regulation. Then two dimensional discretized histograms were made for both buses and the FTP cycle producing three dimensional surface plots similar to the two dimensional intensity images as in Penney et al.[92] Finally, the in-use bus data were compared to the FTP certification cycle using the normalized cross correlation similarity measure *R* (1) where $C_X(i,j)$ is the respective cycle's two dimensional array of operating points.

$$R = \frac{\sum_{(i,j)\in T}(C_{FTP}(i,j)-\bar{C}_{FTP})(C_{Bus}(i,j)-\bar{C}_{Bus})}{\sqrt{\sum_{(i,j)\in T}(C_{FTP}(i,j)-\bar{C}_{FTP})}\sqrt{\sum_{(i,j)\in T}(C_{Bus}(i,j)-\bar{C}_{Bus})}} \qquad 5.1$$

This measure outputs on a value from 1 to -1 with 1 meaning 100% similarity, -1 meaning 100% inverse similarity and 0 meaning no similarity.

NTE Evaluation – The not-to-exceed or NTE emissions testing procedure was designed to measure off-cycle emissions when operating under in-use or real-world conditions. NTE testing is performed on a 30 second or greater segment of in-use data where operating conditions fall within the NTE window. For in-use operation to qualify for certification testing the engine speed must be greater than 15% of max speed; the engine load must be greater than or equal to 30% of max torque; operating points where the engine is producing less than 30% of max power are excluded; the intake manifold pressure (*P*) must relate to intake manifold temperature (*IMT*) and engine coolant temperature (*ECT*) using the equations $P = 0.0875 \times IMT - 7.75$ and $P = 0.0778 \times ECT - 9.8889$; and the exhaust gas temperature must be greater than 250°C within 12 inches of the aftertreatment device to ensure aftertreatment devices are properly warmed.[77] An engine is said to comply with the NTE evaluation when the summation of brake specific NO_X over the test window is less than 1.5 times the FTP emissions limit which 0.401 gNO_X/kWh for the 2010 emissions certification. Equation 5.2 shows the calculation for brake specific NO_X from a desired window.

$$Brake\ Specific\ NO_X\ Emissions\ \left\{\frac{gNO_X}{kWh}\right\} = \frac{(\sum_t grams\ of\ NO_X) * 3600\frac{s}{hr}}{\sum_t Brake\ Power} \qquad 5.2$$

Lagrangian Spatial Analysis – Vehicle drive cycle data are traditionally analyzed by comparing traces of specific vehicle parameters such as speed or emissions over time. However, with the buses performing multiple passes of each route throughout the day, temporal variations in pass duration made cycle to cycle comparison difficult. Therefore,

spatial analysis using GPS data was necessary to properly align asynchronous datasets and provide vital insight into spatio-temporal influences on vehicle operation.

To categorize route and distance along route, the end-of-route regions were identified, or locations in which the buses stopped when transitioning from eastbound to westbound service, using the "within" spatial query. This allowed us to determine the direction of the next route pass. Next, the length and distance from start of the pass were calculated for all road segments comprising each route reducing each route to one dimension. Finally, the GPS coordinates of each data point were matched to a route segment, and the exact distance from beginning of the route was calculated through interpolation. This route matching technique allows for comparison of varying geographic locations using 1-dimensional route distance.

Another difficult aspect when processing GPS data is dealing with slight differences in trajectory and point location from pass to pass. For example, the buses stop at slightly different locations when pulling into a stop, and the GPS records sparser points as the speed increases. With the relatively sparse dataset compared to hypothetical Big Vehicle Data (BVD) consisting of time, location and operational data from all vehicles, it was necessary to bin all the data points and trajectories into 10m increments. When BVD exists, the resolution of this analysis will be able to increase resolution and explore both spatial and temporal aspects of the vehicle data. In contrast to NTE evaluation, the emissions calculated for the Lagrangian Spatial Analysis are provided in grams per kilometer to account for differences in engine power consumption between the hybrid and conventional

bus by shifting to distance specific emissions. Equation 5.3 shows the distance specific emissions calculation.

$$Distance\ Specific\ NO_X\ Emissions\ \left\{\frac{gNO_X}{km}\right\} = \frac{\sum_t grams\ NO_X}{\sum_t Kilometers\ Traveled} \qquad 5.3$$

RESULTS

In-Use Testing: Ambient temperature during the study ranged from -17°F to 90°F, providing a wide range of climates and operating conditions. Over 1200 uniquely identified passes of the route were recorded throughout 66 total days of testing generating nearly 13 gigabytes of spatio-temporal vehicle data. The series hybrid bus data were separated into days with the engine start-stop feature active denoted as Series Hyb. SS and days with the feature turned off denoted as Series Hybrid. Figure 5.2 shows the NO_X emissions in terms of work produced by the engine broken up by bus, climate, and route.

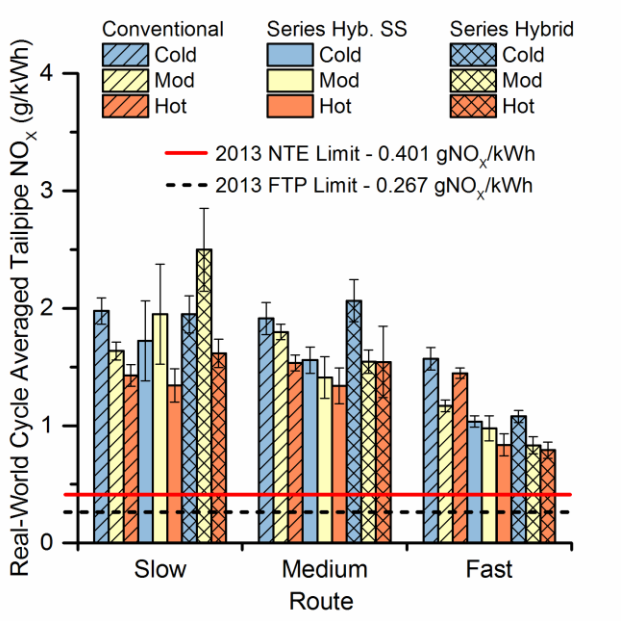

Figure 5.2: Average real-world tailpipe NO_X in g/kWh.

In this instance the hybrid bus performed better on the higher speed routes, and the conventional bus performed better on the low speed route. The use of start-stop in the hybrid bus had little to no statistical change in NO_X emissions compared to the feature being disabled. Due to this finding, all hybrid datasets are combined for further analyses. Despite the expected advantage of the conventional bus for the high-speed route, the hybrid bus required less energy due to its ability to recapture energy through regenerative braking and accessory electrification resulting in lower overall emissions. When the data is presented in grams of NO_X per kilometer, the hybrid emissions are lower for every route. This can be shown in the histograms in Figure 5.3.a where the power consumption factor is removed and the hybrid bus produces fewer grams of tailpipe NO_X emissions per kilometer for all instances. The low speed route had the highest NO_X emissions per kilometer and the highest speed route had the lowest NO_X emissions per kilometer. This supports the findings by [24,82,83] in which slow speed and low load drive produced excessive NO_X for SCR equipped vehicles. Interestingly, both buses on average emitted at rates 3 to 9 times the FTP certification limit of 0.267 gNO_X/kWh under real-world driving conditions. This finding prompted further investigation into the certification status by running the collected data through the NTE test procedure as well as comparing in-use data to the FTP heavy Duty certification cycle.

NTE and FTP Comparison: Using the NTE criteria put forth by federal regulation Title 40 chapter I section 86.1370-2007[77] the collected test data were checked for NTE violations. The broadest limiting NTE requirement is that the exhaust gas temperature must

be 250 °C or greater with 12 inches of the aftertreatment outlet otherwise the NTE test is void as specified in Section G of federal regulation Title 40 chapter I section 86.1370-2007.[77] After examining all recorded instances it was found that the engines never entered an operating range where the engines qualified to be tested under the NTE standard with approximately half of the data being excluded due to the aforementioned exhaust gas requirement. Therefore, despite the recorded high NO_X emissions the buses do not violate their emissions certification since they are never in a qualifying NTE region. A possible explanation for the elevated NO_X emissions could be in part due to the inability of the transit bus to maintain SCR temperature which is crucial for effective NO_X reduction.[93] To verify this, histograms of SCR outlet temperature is shown in Figure 5.3.b.

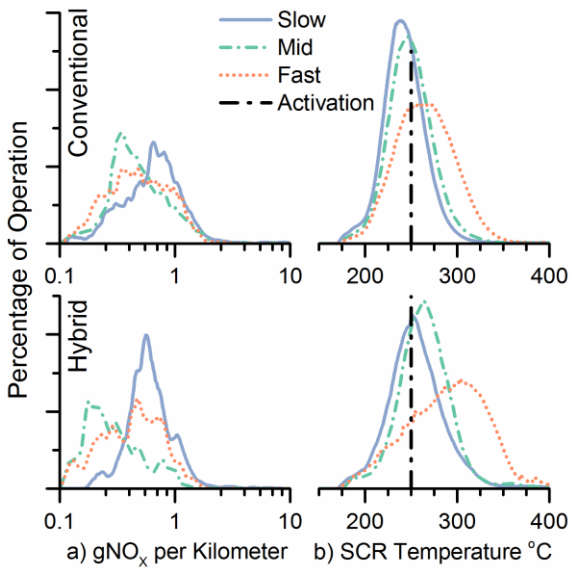

Figure 5.3: Histograms of: a) NO_X emissions and b) SCR outlet temperature

Route kinetic intensity played a major role in the temperature of the aftertreatment system with the lower kinetic intensity routes having higher SCR temperatures on average.

Another factor in SCR temperature was bus type and engine size. The hybrid bus with the smaller 6.7L engine had higher SCR temperatures for similar sets of work indicating the downsized engine was better able to maintain engine temperature. These findings suggest the emissions standard does not accurately regulate in-use transit buses, which is troubling since they make up 7.5%[94] of the heavy duty vehicles this standard was intended for.

To support and quantify the hypothesis that the current test procedures do not accurately portray transit bus operations in practice, the collected test data were compared to the FTP drive cycle by identifying the similarity between frequency distributions of operation ranges. The series hybrid comparison resulted in a 0.13 similarity and the conventional bus resulted in a 0.02 similarity confirming our hypothesis that the FTP certification cycle does not represent transit bus operation. A visual representation of the prescribed FTP cycle operating points as well as in-use operating points of each bus are shown in Figure 5.4. The foci of the FTP cycle are the idle /engine braking conditions making up nearly 38% of operation with the high torque region making up a majority of the remaining operation. Conversely, transit bus operation avoids the high torque region and has relatively less operation time in the idle condition.

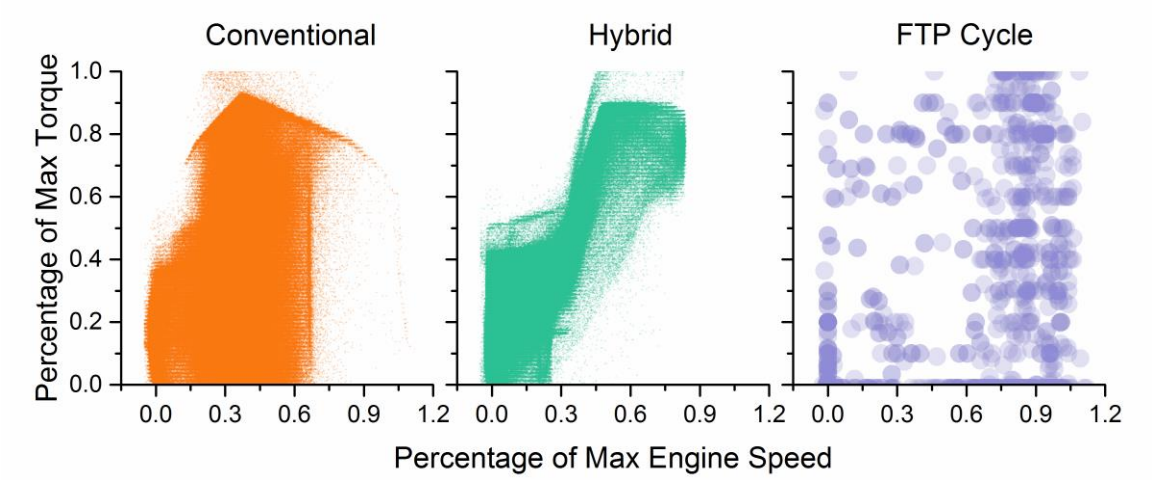

Figure 5.4: Percent maximum torque vs percent maximum engine speed density plots

Lagrangian NOx Hotspots: To examine spatial locations of high NO_X emissions, Lagrangian NO_X hotspots were manually identified by plotting emitted NO_X as a function of location using internally developed software and the mapping program Google Earth. Emissions factor in grams of NO_X per kilometer was chosen for this study to keep consistent with previous plots and the findings by others,[74,95] and consistent with source emissions modeling. However, the Lagrangian hotspot detection technique used here can be applied to any desired vehicle attribute. This analysis provides a unique method for observing and identifying spatial interactions observed by the buses. Spatial NO_X mapping for the conventional diesel bus is shown in Figure 5.5. In the figure, contours are defined based on percentile of NO_X emissions in grams per km for each route given in Figure 5.3.a. Though hotspots could be defined based on any criteria like regulatory emissions values, here NO_X hotspots are defined as regions along a route with emissions above the 97th

percentile. This arbitrary definition allows for ease of comparison between other points along a route as given in the Figure 5.5.

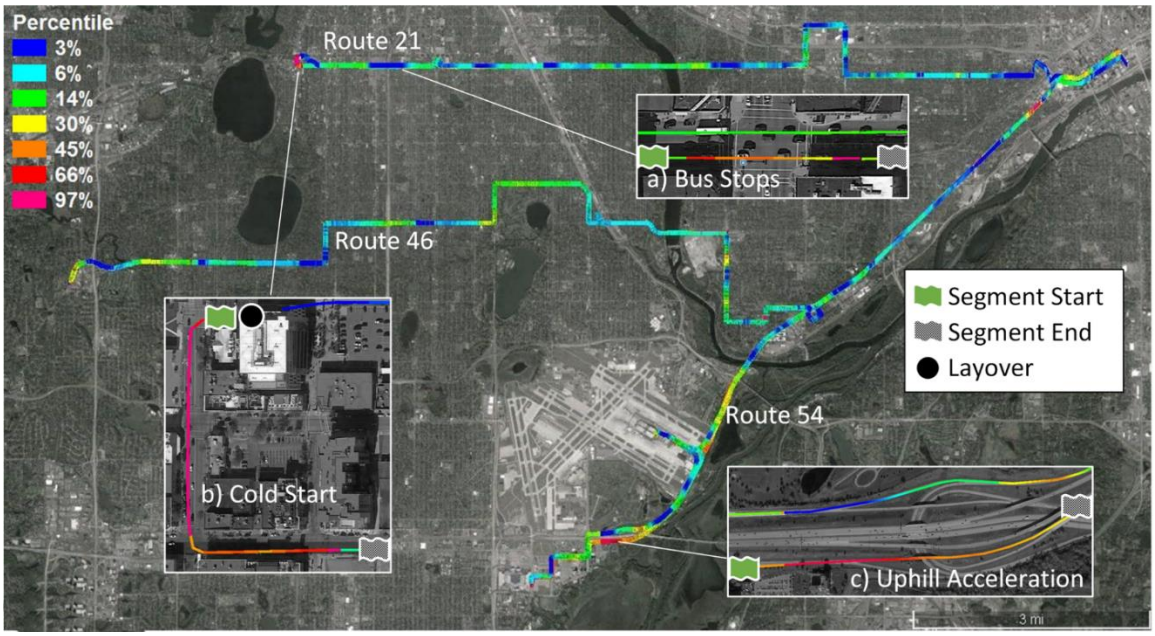

Figure 5.5: Spatial NO_X hotspots for conventional powertrain bus on all three routes. Base Map: Google.

Table 5.1: Vehicle statistics for routes and route segments shown in Figure 4

	Speed (kph)	Bk. Power (kW)	NO_X (g/km)	SCR Temp (°C)	Route
Inset (a)	6.0	25.1	2.11	197	21
Inset (b)	2.5	15.4	6.71	196	21
Inset (c)	71.1	138.4	1.27	234	54
Rt. 21 Avg.	14.8	29.2	0.87	227	21
Rt. 46 Avg.	23.0	34.2	0.60	239	46
Rt. 54 Avg.	26.0	36.4	0.58	213	54

The results indicate that bus stops, cold starts, inclines and accelerations had the most noticeable impact on elevated NO_X emissions for the tested routes. Inset (a) in Figure 5.5

shows an instance where a NO_X emissions hotspot is located in the vicinity of a bus stop and intersection with an average NO_X emissions rate roughly 3.3 times the route average as shown in Table 5.1. This result is supporting by the simulated findings of Gouge et al.[74] where they identified bus stop and intersection emissions to be 1.6 to 3.0 times higher than the route average resulting in a 20% to 40% increase in pedestrian exposure compared to homogeneous emissions distributions. These increases can be attributed to the abundant idle and slow speed conditions experienced around bus stops. Inset (b) shows an instance where the bus finishes one route and starts the next route. The black circle signifies the location of the bus layover or waiting period between the end of one route and the start of the next route. As shown in Table 5.1, emissions rates along the route where the bus begins its next pass are about 2.3 times higher than the route averaged emissions. This can be attributed to poor NO_X conversion resulting from the engine and aftertreatment systems cooling during the route layover.[96] Finally, Inset (c) shows a spatial trajectory with high NO_X emissions as a result of increased fueling in response to the uphill acceleration.

CONCLUSION

The results of this work show that monitoring in-use vehicle emissions from manufacturer installed NO_X sensors can evaluate emissions compliance and determine whether driving cycles are representative of in-use operation. Both transit buses considered in this study were found to be in compliance over a gradient of bus technology, route and ambient temperature because neither bus entered a range or met the NTE criteria where they could be tested. This was a results of certification drive cycles being designed for over

the road trucks with steady, high loads rather than highly transient transit bus operation. It should be noted that this study was limited to one engine manufacturer and model year. Results may vary depending on the age and engine manufacturer. NO_X hotspots from individual vehicles (i.e., Lagrangian hotspots) were identified using spatial analysis techniques to further understand where emissions were multiple times higher than route-averaged values. This ability to determine hotspot magnitude for individual vehicles over a full range of powertrain operation is not possible using existing Lagrangian and Eularian emissions models due to their generalization of vehicle emissions factors and poor spatial resolution.

The data techniques applied here have further implications for manufacturers and policy makers. With ever increasing vehicle connectivity, manufacturers could improve vehicle performance by providing real-time suggestions for augmenting operation based upon spatial hotspot information. While results shown in Figure 5.2 indicate engine start-stop had little impact on overall route NO_X emissions, hypothetically engine start-stop technology could be used to limit human exposure when a series hybrid transit bus enters a known high NO_X location in proximity to a bus stop or location of high population density. For instances of cold start with anticipation of transient driving based on traffic conditions, as in Figure 5.5.b, the bus could preheat its aftertreatment system to allow for effective NO_X reduction. From a regulatory standpoint, spatial analysis could assist with emissions based taxing for certain areas through a practice known as Geo-Fencing whereby different rules are set based upon geographic location.[97] Beyond NO_X emissions, any other

measureable vehicle attribute could be studied using the same Lagrangian methods to identify spatial interactions.

Chapter 6 Reduction of In-Use NOx Emissions from Transit Buses through Management of a Selective Catalytic Reduction System

INTRODUCTION

Mitigation of in-use vehicle emissions is gaining importance given known health and environmental impacts and increasing regulatory scrutiny. The pollutants nitrogen monoxide (NO) and nitrogen dioxide (NO_2), collectively referred to as NO_X, are considered criteria pollutants by global regulatory agencies. When combined with other compounds in the troposphere, they produce particulate matter and ground level ozone [9]. NO_X, especially NO_2, is also harmful on a local scale as direct exposure can produce respiratory inflammation and is harmful to people with asthma [12].

Diesel engines used in medium and heavy-duty vehicle applications are a significant source of NO_X emissions. Strategies for reducing NO_X from diesel engines fall into two main categories. The first is to limit its production during combustion. NO_X formation is proportional to local oxygen concentration and exponentially dependent on combustion temperature through the well-known extended Zel'dovich chemical mechanism. The most common approach to decrease NOx formation rate in an engine is EGR, a process where combustion products are reintroduced into the intake and act as a heat absorbing diluent.

The second NO_X emissions reduction strategy is post-combustion aftertreatment. Since diesel engines operate fuel lean, their exhaust contains excess oxygen; therefore, three way catalysts used in stoichiometric spark ignition engines are not effective. Aftertreatment approaches for NO_X reduction in lean engine exhaust include either absorption, such as a

lean NO_X trap (LNT), or conversion of NO_X to N_2 using SCR. This study focuses on the efficacy of SCR to convert NO_X emissions on transit buses in real-world operation.

An on-highway SCR system is typically integrated into an advanced aftertreatment system that includes several upstream and downstream catalysts, sensors and actuators. The SCR consists of catalytic materials such as copper or iron exchanged zeolites [98] or vanadium and a reductant delivery system for liquid urea-water-solution (UWS) or gaseous ammonia. A sensor upstream of the SCR system measures the incoming NO_X concentration, and the system adjusts the urea injection rate accordingly. After UWS injection, the mixture enters a decomposition reactor where the water evaporates and the resulting urea decomposes into gaseous ammonia (NH_3) and water vapor [99]. The gaseous mixture proceeds to the SCR catalyst where the NH_3 and NO_X react to form N_2 and H_2O. The key reactions for SCR are shown in Equations 1 and 2 [100–102] making it apparent that the stoichiometric ammonia to NO_X ratio (ANR) is 1:1 [103].

$$4NH_3 + 4NO + O_2 \rightarrow 4N_2 + 6H_2O \quad (1)$$

$$4NH_3 + 2NO + 2NO_2 \rightarrow 4N_2 + 6H_2O \quad (2)$$

Exact rates of conversion in SCR systems are dependent on parameters including catalyst temperature, inlet reactant concentrations, species uniformity, and especially NO/NO_2 ratio and catalyst surface storage of NH_3. To achieve target conversion efficiencies and minimize NH_3 slip, ANR is actively controlled through urea dosing and feedback from NO_X and NH_3 sensors in the exhaust system.

The biggest challenge for complete NO_X conversion using SCR systems in real-world or actual use is low temperature performance (< 200°C) [104–107] resulting from cold starts, low load – highly transient duty cycles and heat loss to upstream catalysts, filters and to the environment [108–110]. Low temperature operation leads to insufficient heat for UWS evaporation and decomposition and also limits catalytic activity.

Real-world operation of SCR-equipped heavy-duty engines can result in challenging conditions that lead to higher than desirable NO_X emissions, even though these engines can meet regulatory standards on certification test cycles. Transit bus duty cycles are particularly challenging for NO_X reduction using SCR aftertreatment since they have large durations of low temperature operation and are highly transient compared to regulatory cycles like the FTP. Therefore, in-use NO_X emissions of vocational diesel vehicles like transit buses have been under heavy scrutiny by regulators and the public. Approaches to solve the issue have included increasing heat retention, developing catalyst materials with improved low temperature activity [106–111], enhancing UWS evaporation and flow uniformity, and deploying advanced system monitoring [112] with optimized UWS dosing strategies using model based control algorithms for real-time adjustment [100,113]. Some of these strategies can be implemented through a calibration update and do not require hardware changes, thus allowing for rapid improvements between successive model years and software upgrades for existing vehicles. Despite these known strategies to improve NO_X conversion efficiency, previously published studies[114–119] have only demonstrated

improvements under tightly controlled conditions during engine dynamometer testing with limited application to actual vehicle behavior.

Our own research, as well as others, have shown NO_X control of SCR equipped transit buses to be particularly challenging due to the highly transient drive cycle, slow speed and low load driving, cool exhaust temperatures and frequent cold starts [20,24,106,120]. Though these studies have convincingly illustrated that real-world NO_X emissions are elevated for challenging transit bus-like driving cycles, very few have offered solutions for solving the technical challenges necessary to reduce emissions under these conditions. This work shows how continuous improvements to SCR systems can lead to significant emissions reductions by comparing a 2013 model year (MY) SCR-equipped transit bus with a 2015MY bus under real-world driving conditions using original equipment manufacturer installed NO_X sensors and the bus CAN. Both buses are required to meet the same emissions regulations; however, the 2015MY bus had an updated SCR system that included both hardware and control software changes meant to improve in-use NO_X emissions.

EXPERIMENTAL METHODS

Test Vehicle Selection: Two GILLIG forty-foot transit buses were used as the test vehicles for this study. Both buses had conventional (non-hybrid) drivetrains, automatic transmissions, electric cooling fans and Cummins ISL 8.9L diesel engines certified to the 2013 EPA and CARB emissions standards [121]. For NO_X, the certification limit is 0.267 gNO_X/kWh (0.2 g/bhp-hr) over the FTP heavy-duty transient dynamometer cycle. In

addition the standard prescribes NTE emission caps for a specified range of engine speed and load combinations that do not follow the FTP cycle.

Emissions reduction technologies employed on each bus included a diesel oxidation catalyst, DPF, SCR system and EGR. A diagram of the aftertreatment system is shown in Figure 6.1. The difference between the two buses comes in their model year and SCR system improvements described in the next section. The 2013MY bus is the same bus used in our previous study where we reported elevated real-world NO_X emissions [120]. At the start of this study, the 2013MY bus had accumulated 81,300 miles and the 2015MY had 14,200 miles on it with roughly 2,000 miles added per bus throughout the test period.

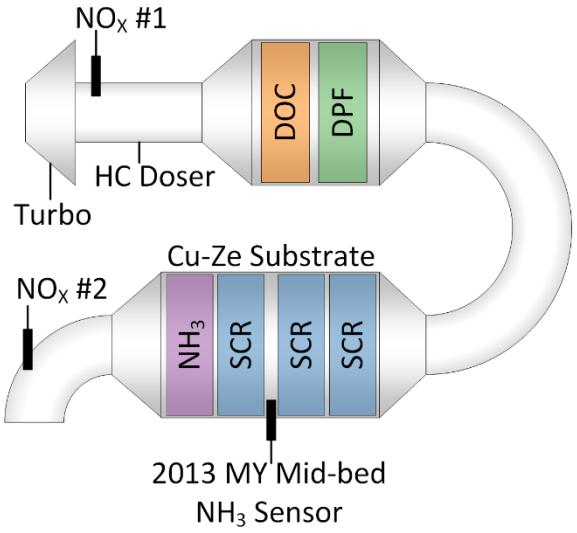

Figure 6.1: Cummins ISL aftertreatment diagram for 2013 and 2015MY buses illustrating location of mid-bed NH_3 sensor for 2013MY bus. Adapted from Stanton 2013[122]

SCR systems: The SCR systems used in both buses shown in Figure 6.1 consist of a catalyst with copper-zeolite coating and a downstream ammonia oxidation catalyst (slip catalyst) for NH_3 catalysis. A NO_X sensor located at the exhaust turbine outlet (NO_X #1) is used to compute a feedforward dosing command to the UWS injector, and a NO_X sensor located at the exit of the SCR system (NO_X #2) is used to ensure conversion is within acceptable limits. An additional mid-bed NH_3 sensor is present in the 2013MY SCR system to assess NH_3 storage on the catalyst and adjust dosing accordingly. The newer SCR system on the 2015MY bus is not equipped with a NH_3 sensor but instead uses model-based control software to anticipate catalyst storage.

Instrumentation: NO_X measurements were performed using the stock vehicle NO_X sensors, located at the turbine outlet and at the tailpipe downstream of the aftertreatment system (see Figure 6.1). These sensors communicate information with the engine control module across the heavy-duty vehicle J1939 CAN. The NO_X sensors are used in SCR control to direct UWS dosing and to diagnosing aftertreatment system faults. The specified sensor accuracy is ±10ppm from 0 to 100ppm and ±10% from 100ppm to 2000ppm [91]. SCR inlet and outlet temperature was measured by the stock thermistors while exhaust flow rate and engine power were estimated by the ECM. These data were collected using a National Instruments cRIO-9074 controller and NI-9853 CAN module. Location information and wireless data transfer were provided using a S.E.A Cellular GPS module. Data were sent to the University of Minnesota for storage and spatial post processing in a MySQL database.

Electrochemical NO_X sensors are known to be cross-sensitive to NH_3, therefore the tailpipe NOx reading may be confounded by the presence of NH_3 from UWS injection [123–125]. To address possible interference from sensor cross-sensitivity to NH_3 and quantify sensor accuracy, a small subset of the test period involved portable emissions measurement system (PEMS) equipment that incorporated a non-dispersive infrared analyzer. This short study compared the time traces of the CAN NO_X sensors to the NO_X measurement from certified PEMS equipment. A sample of this data is shown in Figure 6.2 to illustrate the differences between the PEMS and J1939 NO_X measurement in both transient and idle situations.

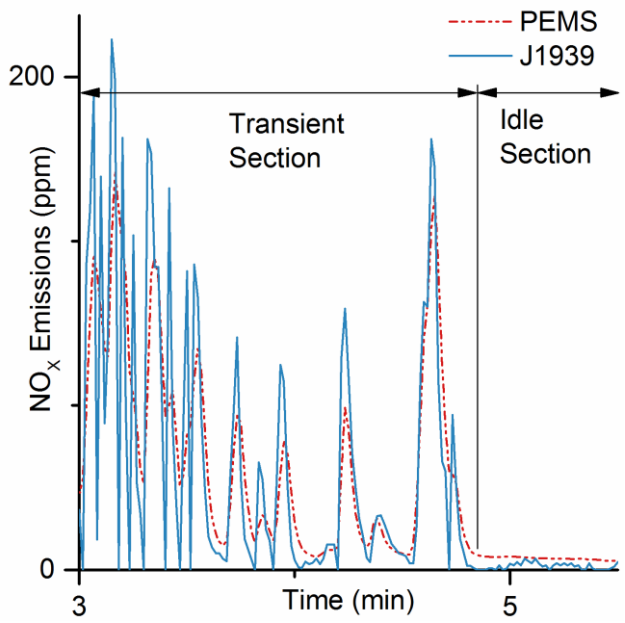

Figure 6.2: Comparison of PEMS NO_X measurement to J1939 CAN NO_X sensor measurement for transient and idle periods.

Results from the comparison test indicated that the NO_X sensor had comparable accuracy and better response time than the instrument grade analyzer, indicating that cross-sensitivity was not a particular concern in for our study.

Test route selection: This study used the same slow, medium and fast routes as described in Chapter 2 as used in our previous work [120], which capture a wide range of transit bus operation. Generating over 250 hours of combined data collected at 1 Hz, the buses were tested for 9 days running approximately 14 hours per day. The ambient temperature range during the data collection period was 13°C to 32°C.

Data analysis:

Cycle Average Comparison – The first analysis was a high-level, cycle average comparison that evaluated emission rates based on the average of each pass. To identify unique passes throughout the day, spatial algorithms were used to isolate end-of-route regions from the GPS information with a new pass being defined as the data from the event series of a bus entering an end-of-route region, exiting the region and immediately prior to reentering the next region. Next, the average tailpipe NO_X emission in gNO_X/kWh, engine out NO_X emissions gNO_X/kWh, ammonia to NO_X ratio (ANR) and brake specific power (P_{Brake}) in kW for each pass were calculated to generate one data point per pass. To account for each pass having slightly different real-world characteristics based on traffic, frequency of stops and ridership, mean values and 95^{th} percentile error bars are reported.

Intensity Analysis – The dependence of tailpipe NO_X and ANR were examined as a function of the time derivative of engine brake power ($\dot{P}_{Brake}$), SCR temperature (T_{SCR}) and

engine out NO_X. Gathered raw CAN data were post-processed and then each 1 Hz data point was analyzed using intensity scatter plots. $\dot{P}_{Brake}$ was calculated as the time derivative of brake power (P_{Brake}) based on the summation of ECM-calculated engine power (P_{Engine}) and frictional loss power ($P_{Friction}$) shown in Equations 2 and 3. The engine frictional powers were calculated based on the SAE J1939 standard [126].

$$\dot{P}_{Brake} = \frac{dP_{Brake}}{dt} \quad (2)$$

$$P_{Brake} = P_{Engine} - P_{Friction} \quad (3)$$

SCR catalyst temperature was calculated using an average between the measured SCR catalyst inlet and outlet temperatures shown Equation 4, and engine-out NO_X concentration in ppm remained as reported from the CAN.

$$T_{SCR} = \frac{T_{SCR\ Inlet} + T_{SCR\ Inlet}}{2} \quad (4)$$

After processing the data, each point was placed on a two dimensional scatter plot resulting in a quasi-3D intensity plot based on intensity of the data points meaning frequent points show up darker than less frequent points.

RESULTS AND DISCUSSION

Cycle-Averaged Emissions Results: Figure 6.3 shows cycle averaged parameters, broken down by route, providing a high level overview of our study. Figure 6.3.b and Figure 6.3.d show that there was no statistical difference in the engine out NO_X or brake power, however Figure 6.3.a shows that the 2015MY bus achieved an 80% reduction in real-world, cycle average tailpipe NO_X emissions over the 2013MY bus.

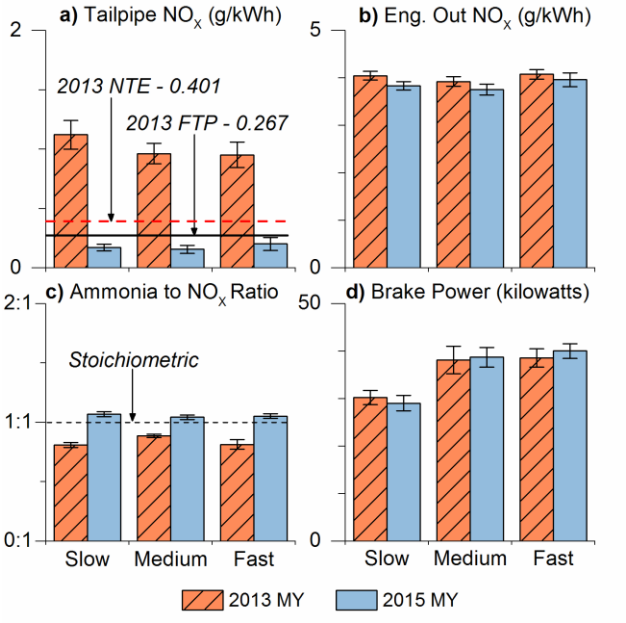

Figure 6.3: Cycle averaged data for the 2013 and 2015MY transit buses on three routes of increasing average route speed: a) tailpipe NO_X emissions, b) engine-out NO_X emissions, c) ammonia to NO_X ratio, and d) engine brake power.

The only other notable difference between the model years was the near 25% increase in ANR for the 2015MY bus as shown in Figure 6.3.c. These findings were verified with Metro Transit's records, which indicate an 18% increase in average UWS consumption between the 2013 and 2015MY buses. This indicates that the NO_X reduction in the 2015MY bus is attributable to increased effectiveness of the SCR exhaust aftertreatment.

Directed Analysis of Emissions Reduction: Although the cycle-averaged tailpipe NO_X emissions from the 2015MY bus were significantly lower than the 2013MY bus on the three tested routes, it is of interest to study the cause of this reduction and determine under which driving conditions the improvements were made. Here, the response of tailpipe NO_X emissions and ANR to changes in $\dot{P}_{Brake}$, T_{SCR} and engine-out NO_X is

examined for the two transit buses using intensity plots. Areas of frequent operation appear darker and points with less frequent operation appear lighter providing a quick visualization of how often each bus operated in a particular area.

Transient Power – The system behavior as a function of the time derivative of engine brake power, $\dot{P}_{Brake}$ in kW/s, reflects the SCR aftertreatment system's transient performance. Figure 6.4 provides a plot of $\dot{P}_{Brake}$ versus NO_X emissions and ANR. Data points where $\dot{P}_{Brake} > 0$ indicate system response to increasing power and likewise values of $\dot{P}_{Brake} < 0$ denote system response to decreasing power. For the tailpipe NO_X plots in Figure 6.4, both MY buses have a vertical line centered at $\dot{P}_{Brake} = 0$ indicating the NO_X emitted and ANR at steady state conditions. For non-steady state conditions or $\dot{P}_{Brake} \neq 0$, the 2013MY bus had higher NO_X emissions, which is expected based on the route averaged data shown in Figure 6.3.

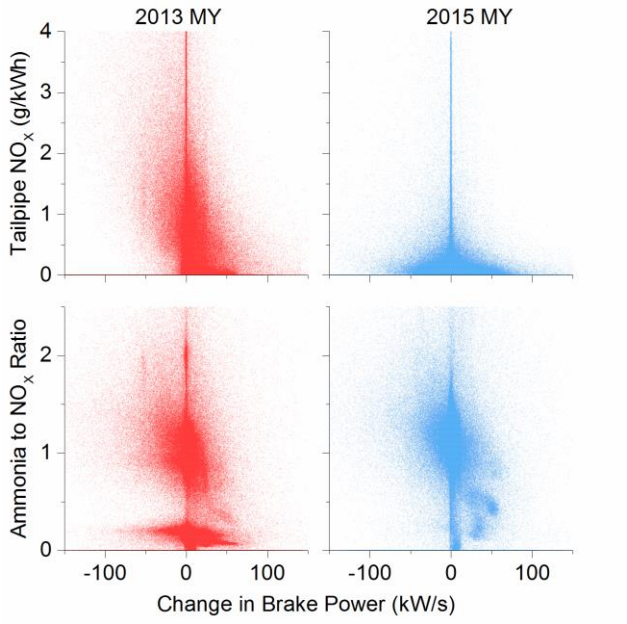

Figure 6.4: Tailpipe NO_X and ANR vs change in engine brake power output.

The notable difference between the two buses can be seen for $\dot{P}_{Brake} < 0$. For the 2015MY bus, tailpipe NO_X emissions on either side of $\dot{P}_{Brake} = 0$ decreased indicating an active system response to transient events. Conversely, the 2013MY bus shows decreasing NO_X emissions for $\dot{P}_{Brake} > 0$ and increasing emissions for $\dot{P}_{Brake} < 0$ indicating a poor SCR system response to negative $\dot{P}_{Brake}$. This difference is a contributing factor in elevating the NO_X emissions of the 2013MY bus as instances of negative $\dot{P}_{Brake}$ frequently occur. Examples include the bus decelerating, the vehicle attaining cruising speed or when the transmission momentarily disengages from the engine during gear shifts.

SCR Temperature – One of the most important factors in SCR operation is catalyst temperature. At temperatures below 200°C UWS evaporation becomes difficult and catalyst activity is poor. At high temperatures such as those induced from active regeneration of the DPF (>500°C), NH_3 may be oxidized to NO_X within the SCR system. The plot of NO_X dependence on SCR catalyst temperature in Figure 6.5 shows similar results to the previous plots where the 2013MY bus had higher overall tailpipe NO_X emissions than the 2015MY bus.

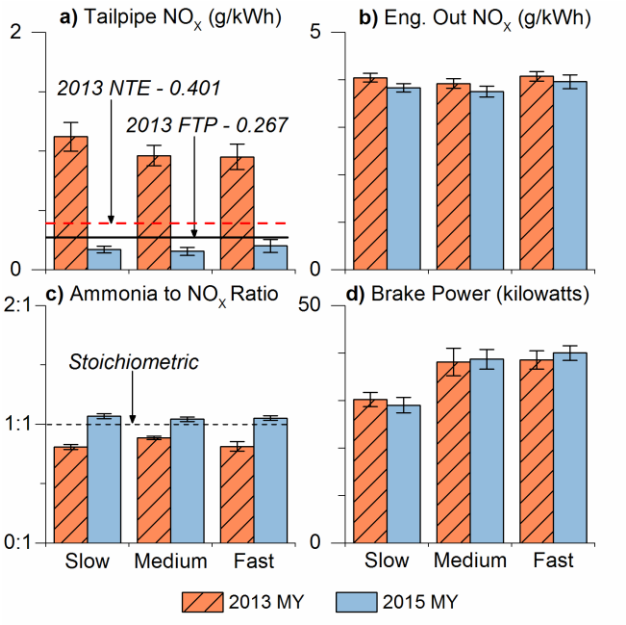

Figure 6.5: Tailpipe NO_X and ANR vs SCR catalyst temperature with 0.2% dosing lines indicating major dosing onset temperature and the centroid providing the mean value of all data.

Apart from those previously established results, a noticeable finding from these plots is that the 2013MY bus had decreasing tailpipe NO_X emissions with increasing SCR catalyst temperatures from 180°C and 350°C, whereas the 2015MY bus had relatively constant emissions with varying bed temperature. Furthermore, the plots of ANR as a function of catalyst temperature in Figure 6.5 show the deviation across the catalyst temperature range providing insight into the UWS dosing strategies used as a function of catalyst temperature. The 2015MY bus exhibited a singular control area with ANR values between 0.8 and 1.5 and a slight inverse correlation of ANR and catalyst temperature. However, the 2013MY plot reveals a pronounced difference with 5 primary horizontal ANR bands for the same temperature ranges as well as a larger range of ANR values

between 0.2 and 2. This illustrates that the SCR control strategy in the 2013MY bus had discrete ANR levels without precise gradient control for a large range of operation, a feature not apparent in the 2015MY bus data. Further, the large band centered on 0.2 ANR and the lower centroid for the 2013MY may explain some of the elevated NO_X emissions due to the limited amount of ammonia available to perform the SCR reaction.

Engine-Out NO_X – Tailpipe NOx emissions are highly dependent on the inlet reactant concentrations. Figure 6.6 gives an intensity plot of tailpipe NO_X and ANR as a function of engine-out NO_X providing a graphical view of in-use SCR conversion efficiency for the two buses.

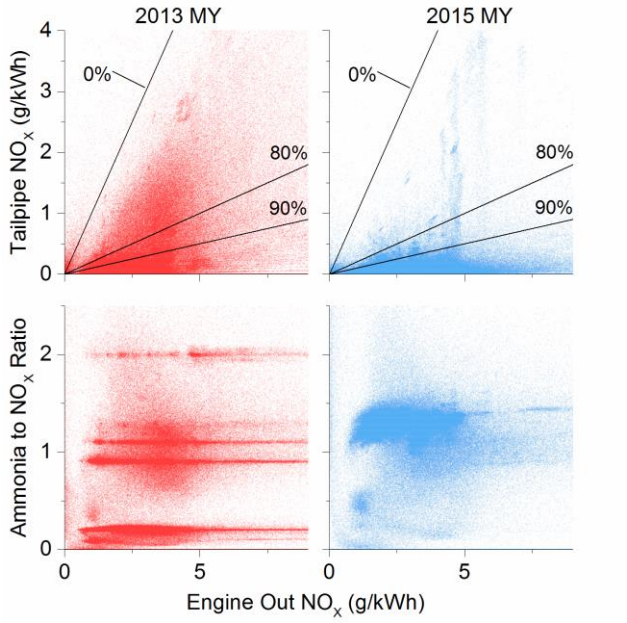

Figure 6.6: Tailpipe NO_X and ANR vs engine out NO_X with 0%, 80% and 90% conversion lines.

Lines of NO_X conversion efficiency are provided with the 0% line meaning no conversion and the x-axis equaling 100% conversion. While the plots of tailpipe NO_X in

Figure 6.6 show similar results to the previous figures, it is interesting to note that the 2013MY bus tailpipe NO_X drops below the 80% conversion line whereas the 2015MY has a relatively constant tailpipe NO_X. For the plots of ANR, the 5 different bands of dosing are again present for the 2013MY, while the 2015MY has a single large band. However, each of the bands cross the length of the plot for the 2013MY bus signifying distinct dosing levels between 0.2 and 2 ANR are all possible for every level of engine out NO_X, whereas the 2015MY bus has the single band around 1.25 ANR which is closer to stoichiometric ammonia – NO_X reaction.

2013 SCR System Retrofit Study: We conducted an additional study examining NO_X emissions from the same 2013MY bus as used in the main study following a replacement of its stock SCR system with a 2015MY SCR system. Once repairs were complete, the 2013MY bus which is denoted as "2013 repaired" was re-evaluated on the same routes, but during the winter or "cold" season with temperatures ranging from -21°C to 7°C. Results shown in Figure 6.7 indicate increased ANR for the 2013 replacement is similar to that of the 2015MY bus.

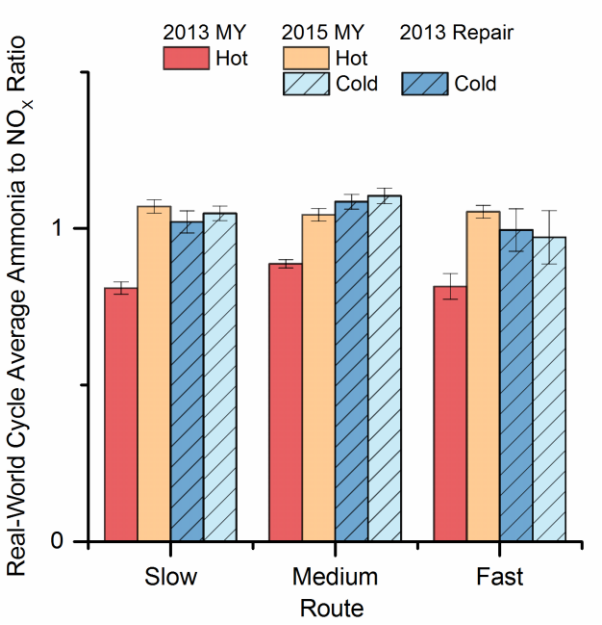

Figure 6.7: Ammonia to NO_X ratio comparison for cold and hot seasons with the 2013MY, the same 2013MY after SCR repair and the 2015MY bus.

The real-world cycle averaged NO_X emission for the replacement system are shown in Figure 6.8. Results show a substantial reduction in real-world NO_X emissions similar to that seen in the 2015MY bus and confirm that the aftertreatment hardware and software changes, and not engine characteristics, are the reason for the reduction.

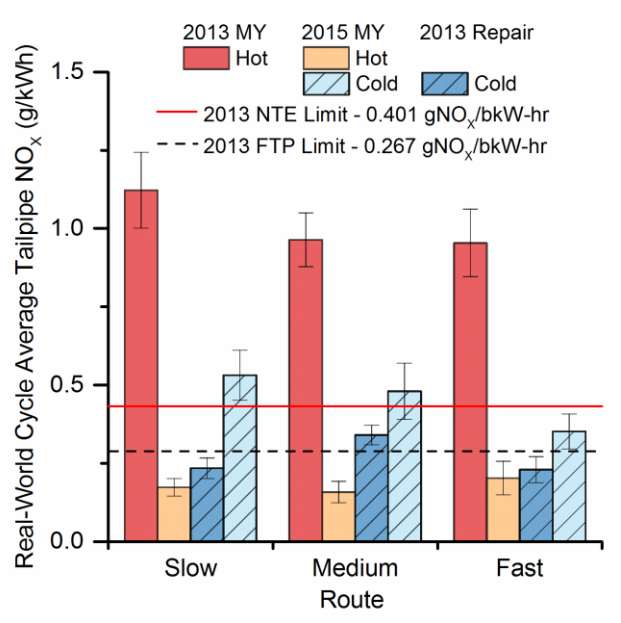

Figure 6.8: Tailpipe NO_X emissions comparison for cold and hot seasons with the 2013MY, the same 2013MY after SCR repair and the 2015MY bus.

Additional Analysis: While our study shows that changes to dosing strategy were instrumental to improving in-use NO_X emissions, other system changes also helped enable these improvements. As the primary challenge to exhaust aftertreatment related to maintaining proper temperature adherence, improving insulation can help shorten system heat-up time thus reducing cold-start emissions and increase downstream exhaust temperatures for better SCR system operation. Lowering the dosing onset temperature is another way to reduce cold start emissions with UWS evaporation and conversion to NH_3 being the primary challenge to overcome. For the 2013MY bus the lowest temperature where dosing activity was recorded was 115.9°C, whereas the 2015MY bus was able to dose at 92.9°C. However, this improvement had minimal impact as shown in Figure 6.5 where 0.2% of measured dosing was reached at roughly 180°C meaning the remaining

99.8% of dosing occurred at temperatures at or above 180°C. A key method for increasing the effectiveness of NO_X conversion is to optimize flow and NH_3 uniformity across the SCR substrate inlet, improving NO_X reduction while reducing NH_3 slip. In an ideal dosing situation the exact amount of UWS would be injected and converted into NH_3 to stoichiometrically convert all of the inlet NO_X into harmless products, however with complex chemical kinetics, transient exhaust flow rates and intricate vehicle packaging requirements this is not possible. To overcome these challenges, computational fluid dynamics[112,127] has been performed to understand UWS injection characteristics such that design changes can be made to optimize catalyst coating uniformity or identify how overdosing (ie. ANR >1.0) could increase NO_X conversion.

These findings provide great promise towards mitigation of excessive vehicle NO_X emissions. For example, if 150 of Metro Transit's 2013MY bus engines were retrofitted with 2015MY aftertreatment systems, and assuming each bus runs 10 hours a day for 5 days a week over a cycle similar to those identified in this paper, 11,000 kg of NO_X could be eliminated from entering the atmosphere each year. Extending these findings to older model year transit buses and other diesel vehicles, the improvements in real-world NO_X emissions demonstrated here could have substantial positive impact on both air quality and the environment.

CONCLUSION

The improvement in SCR aftertreatment technology between the 2013 and 2015MY buses shown here is a result of a continuous research and development process. While the

improved control and increased dosing have provided substantial reductions, many parts of the system have also been upgraded including improved thermal insulation, lowered dosing onset temperature through improved catalysts and optimized fluid dynamics during UWS injection though the effects of these upgrades were not directly studied here. It is likely that other transit buses and vocational vehicles will express different characteristics based on their specific operating conditions; however, researchers and aftertreatment manufacturers can use the results presented in this work as evidence that SCR system improvements can reduce in-use NO_X emissions, even under demanding operating conditions like transit bus duty cycles. Further, the in-use emissions of older vehicles can be improved through retrofitting.

Chapter 7 Future Work

The research presented here provides the groundwork for future studies with particular applications in passenger counting, and connected and automated vehicles described below.

MASS BASED AUTOMATIC PASSENGER COUNTER

Based on this initial investigation, further refinement of mass-based APC is warranted. Future work will involve instrumenting a variety of buses including coach and articulated vehicles. Development of data processing algorithms will be a key focus to improve accuracy and address the issue of misreads during kneeling for our mass-based APC technology. More data collection will be necessary to properly categorize boarding/alighting events and non-events. Various machine learning algorithms or dynamic models may be appropriate for identifying unique event cases.

VEHICLE NO_X EMISSIONS

Based on the NO_X reduction results presented in Chapter 6, future actions could entail extending the vehicle retrofit study to more vocational vehicles, architectures and model years. For 2007 and later model year heavy duty vehicles that have SCR aftertreatment, it is likely that a retrofit would be possible with current emissions levels being phased in from 2007 to 2009 and fully present starting in 2010 [128]. With roughly 1000 vehicles in the Metro Transit bus fleet and a 12-year turnover requirement for federal subsidies, this would roughly equate to 580 vehicles assuming an even distribution throughout the model years. Using the estimates from Chapter 6 and assuming all of the 580 buses emit at levels equal

to that of the 2013MY, this could equate eliminate roughly 170,000kg of NO_X from entering the atmosphere over the next 4 years. Furthermore, with the 2013MY being 6 years newer than the 2007MY vehicles, it is likely that the NO_X reduction from retrofit would be larger.

CONNECTED VEHICLES

Connected vehicles with enhanced sensor quality, low data storage costs and improved computing power will enable Lagrangian emissions analyses to be performed at a larger scale and with ever increasing accuracy. Taken to the extreme, spatial emissions from a statistically significant number of vehicles on a roadway at a given time could be monitored and combined to form a more accurate Eularian description of traffic flow and emissions than stationary monitoring sites. However, with over 250 million vehicles registered in the U.S.[94] each producing hundreds of spatially tagged parameters each second, collecting even one day of second by second data would produce roughly 90 trillion entries. The sheer size of data possible as more vehicles are connected presents a significant challenge to extending Lagrangian analyses. Spatial big data techniques such as those employed in routing applications where directions are calculated based on previous journeys and real time traffic information[129,130] will be required. I have publically advocated for future vehicle research[131,132] to focus on spatial big data techniques for better understanding connected vehicle emissions from the Lagrangian frame of reference. These new tools can effectively bridge the critical gap between Eularian monitoring and vehicle emissions modeling to accurately quantify emissions from in-use vehicles at high spatial resolution.

Such analysis and testing techniques would reduce the need for dynamometer certification, and with the advent of connected vehicles and low cost sensors, could be performed continuously on fleet-wide scale enabling a collective gathering of knowledge to rapidly develop and improve vehicle performance. Aberrant vehicles operating outside of the desired operating ranges could be quickly identified and studied allowing manufactures to decide corrective measures prior to vehicle breakdown or cost to their customers. Further, rapid identification would benefit society in being able to assess exact emissions sources and understand where the biggest reduction potentials are allowing research efforts to be focused accordingly.

One known caveat to big data analysis is the propensity for false positive outcomes resulting in correlations that disobey physical laws or have no physics based relation. To address this issue physics aware data mining methods should be developed which uses physical models during analysis to reduce false outcomes and further develop the area specific knowledge. Such improvements could embody developing a physics-aware spatiotemporal data model of vehicle NO_X emissions based on various input parameters including location, climate, vehicle mass, engine age, maintenance status and system operational parameters known as physics aware spatiotemporal data analysis (PSDA). Using cloud-based computing and vehicle connectivity these developed to improve vehicle performance. Taken to the extreme, every vehicle would have connectivity and could use information provided from other vehicle's traversal of a route to optimize their own operation similar to methods used for suggesting related items for online purchases on

websites like Amazon.com. These optimizations could present in the form of suggestions to allow the user full control over their vehicle. Using the series hybrid transit bus data collected throughout these works, I estimate a vehicle fleet collective fuel economy improvement of 18% through battery state of charge, engine operation and routing optimizations providing substantial benefit with minimal added cost. This can be tested using a small subset of a transit bus fleet placed on the same route. The circulation of connected transit buses on a high-frequency inner-city route would provide an ideal use-case for testing real-time optimization using V2X connectivity and PSDA algorithms due to the repetitive nature, diverse traffic conditions and proximity to other V2X equipped vehicles.

Bibliography

(1) Melillo, J. M.; Richmond, T.; Yohe, G. W. *Climate Change Impacts in the United States: The Third National Climate Assessment*; 2014.

(2) US EPA Climate Change Division. Greenhouse Gases Overview http://www.epa.gov/climatechange/ghgemissions/gases.html (accessed Dec 11, 2014).

(3) US EPA; OAR; OAQPS. Air Pollution Emissions Overview http://www.epa.gov/airquality/emissns.html (accessed Dec 1, 2014).

(4) U.S. Environmental Protection Agency. *Inventory of U. S. Greenhouse Gas Emissions and Sinks : 1990 - 2012*; Washington, DC, 2014.

(5) Dlugokencky, E.; Tans, P. ESRL Global Monitoring Division - Global Greenhouse Gas Reference Network http://www.esrl.noaa.gov/gmd/ccgg/trends/global.html (accessed Nov 28, 2014).

(6) Ackerman, F.; Stanton, E. a. Climate Risks and Carbon Prices: Revising the Social Cost of Carbon. *Econ. Open-Access, Open-Assessment E-Journal* **2012**, *6*, 0–26.

(7) Sundquist, E.; Burruss, R.; Faulkner, S.; Gleason, R.; Harden, J.; Kharaka, Y.; Tieszen, L.; Waldrop, M. Carbon Sequestration to Mitigate Climate Change. *US Geol. Surv.* **2008**, No. December, 1–4.

(8) Turns, S. R. *An Introduction to Combustion: Concepts and Applications*, 3rd ed.; Lange, M., Stenquist, B., Neyens, L., Eds.; Raghothanman Srinvasan: New York, NY, USA, 2012.

(9) Grewe, V.; Dahlmann, K.; Matthes, S.; Steinbrecht, W. Attributing ozone to NOx emissions: Implications for climate mitigation measures. *Atmos. Environ.* **2012**, *59* (x), 102–107.

(10) Southworth, F.; Meyer, M. D.; Weigel, B. A. *TRANSIT GREENHOUSE GAS EMISSIONS MANAGEMENT COMPENDIUM*; FTA-GA-26-7006.2011.01; Atlanta, GA, 2011.

(11) US EPA. Ground Level Ozone Health Effects http://www.epa.gov/groundlevelozone/health.html (accessed Nov 30, 2014).

(12) US EPA; OAR; OAQPS. Health | Nitrogen Dioxide | US EPA http://www.epa.gov/airquality/nitrogenoxides/health.html (accessed Dec 1, 2014).

(13) Vijayaraghavan, K.; Lindhjem, C.; DenBleyker, A.; Nopmongcol, U.; Grant, J.; Tai, E.; Yarwood, G. Effects of light duty gasoline vehicle emission standards in the United States on ozone and particulate matter. *Atmos. Environ.* **2012**, *60*, 109–120.

(14) Office of Transportation & Air Quality. *MPG: Label Values vs. Corporate Average Fuel Economy (CAFE) Values Label MPG*; 2014.

(15) Jackson, T. R. *Fleet Characterization Data for MOBILE6 : Development and Use of Age Distributions , Average Annual Mileage Accumulation Rates , and Projected Vehicle Counts for Use in*; 2001.

(16) NHTSA. *Summary of Fuel Economy Performance*; Washington, DC, 2013.

(17) Administration, F. H. *ANNUAL VEHICLE DISTANCE TRAVELED IN MILES AND RELATED DATA - 2011*; Wahington, DC, 2013.

(18) Office of Energy Statistics. *Monthly Energy Report*; Washington, DC, 2014.

(19) Federal Highway Administration. *ANNUAL VEHICLE DISTANCE TRAVELED IN MILES AND RELATED DATA - 2008*; Wahington, DC, 2011.

(20) Wu, Y.; Zhang, S. J.; Li, M. L.; Ge, Y. S.; Shu, J. W.; Zhou, Y.; Xu, Y. Y.; Hu, J. N.; Liu, H.; Fu, L. X.; et al. The challenge to NO_x emission control for heavy-duty diesel vehicles in China. *Atmos. Chem. Phys.* **2012**, *12* (19), 9365–9379.

(21) Huo, H.; Yao, Z.; He, K.; Yu, X. Fuel consumption rates of passenger cars in China: Labels versus real-world. *Energy Policy* **2011**, *39* (11), 7130–7135.

(22) Boriboonsomsin, K.; Barth, M. Impacts of Road Grade on Fuel Consumption and Carbon Dioxide Emissions Evidenced by Use of Advanced Navigation Systems. *Transp. Res. Rec. J. Transp. Res. Board* **2009**, *2139*, 21–30.

(23) Boriboonsomsin, K.; Scora, G.; Barth, M. Analysis of Heavy-Duty Diesel Truck Activity and Fuel Economy Based on Electronic Control Module Data. *Transp. Res. Rec. J. Transp. Res. Board* **2010**, *2191* (1), 23–33.

(24) Misra, C.; Collins, J. F.; Herner, J. D.; Sax, T.; Krishnamurthy, M.; Sobieralski, W.; Burntizki, M.; Chernich, D. In-Use NOx Emissions from Model Year 2010 and 2011 Heavy-Duty Diesel Engines Equipped with Aftertreatment Device. *Environ. Sci. Technol.* **2013**, *47*, 7892–7898.

(25) Barkenbus, J. N. Eco-driving: An overlooked climate change initiative. *Energy Policy* **2010**, *38* (2), 762–769.

(26) Barth, M.; Boriboonsomsin, K. Real-World Carbon Dioxide Impacts of Traffic

Congestion. *Transp. Res. Rec. J. Transp. Res. Board* **2008**, *2058* (1), 163–171.

(27) Baltusis, P. On Board Vehicle Diagnostics. *SAE Tech. Pap. 2004-21-0009* **2004**.

(28) Reza, R. 2010 Audi A4: The Car With The Sixth Sense http://www.carthrottle.com/2010-audi-a4-the-car-with-the-sixth-sense/ (accessed Dec 9, 2014).

(29) Ford. OpenXC || Ford Developer Support https://developer.ford.com/pages/openxc.

(30) National Highway Traffic Safety Administration (NHTSA). U.S. Department of Transportation Announces Decision to Move Forward with Vehicle-to-Vehicle Communication Technology for Light Vehicles http://www.nhtsa.gov/About+NHTSA/Press+Releases/2014/USDOT+to+Move+Forward+with+Vehicle-to-Vehicle+Communication+Technology+for+Light+Vehicles (accessed Dec 9, 2014).

(31) Deutsch, C. H. U.P.S. Embraces High-Tech Delivery Methods. *New York Times*. Louisville, KY July 2007.

(32) Davenport, T. H.; Dyche, J. Big Data in Big Companies. International Institute for Analytics 2013, pp 1–31.

(33) Tan, P. N.; Steinbach, M.; Kumar, V. *Introduction to Data Mining*; Goldstein, M., Harutunian, K., Eds.; Addison-Weseley: Boston, MA, 2006.

(34) Shekhar, S.; Chawla, S. *Spatial Databases: A Tour*; Holm, T. D., O'Brien, V., Trentacoste, C., Donovan, P., Dulles, G., Eds.; Prentice Hall, Inc.: Upper Saddle

River, NJ, 2003.

(35) Yuan, J.; Zheng, Y.; Zhang, C.; Xie, W.; Xie, X.; Sun, G.; Huang, Y. T-drive: driving directions based on taxi trajectories. In *Proc. of the SIGSPATIAL Intl. Conf. on Advances in GIS*; GIS '10; 2010; pp 99–108.

(36) Fawcett, J.; Robinson, P. Adaptive routing for road traffic. *Comput. Graph. Appl. IEEE* **2000**, *20* (3), 46–53.

(37) Pu, J.; Liu, S.; Qu, H.; Ni, L. Visual Fingerprinting : A New Visual Mining Approach for Large-Scale Spatio-temporal. In *Advanced Data Mining and Applications*; 2012; pp 502–515.

(38) Li, X.; Han, J.; Lee, J. G.; Gonzalez, H. Traffic density-based discovery of hot routes in road networks. *Adv. Spat. Temporal Databases* **2007**, 441–459.

(39) Won, J. I.; Kim, S. W.; Baek, J. H.; Lee, J. Trajectory clustering in road network environment. In *Computational Intelligence and Data Mining, 2009. CIDM'09. IEEE Symposium on*; 2009; pp 299–305.

(40) Shekhar, S.; Lu, C. T.; Zhang, P. A unified approach to detecting spatial outliers. *Geoinformatica* **2003**, *7* (2), 139–166.

(41) Shekhar, S.; Evans, M. R.; Kang, J. M.; Mohan, P. Identifying patterns in spatial information: A survey of methods. *Wiley Interdisc. Rew. Data Min. Knowl. Discov.* **2011**, *1* (3), 193–214.

(42) Campbell, J.; Watts, W.; Kittelson, D. Reduction of Accessory Overdrive and Parasitic Loading on a Parallel Electric Hybrid City Bus. *SAE Int. 2012-01-1005*

2012.

(43) Charmley, W. J. The Federal Government's Role in Reducing Heavy Duty Diesel Emissions. *SAE Int. 2004-01-2708* **2004**.

(44) US EPA Office of Transportation and Air Quality. On-Board Diagnostics (OBD) http://www.epa.gov/obd/regtech/heavy.htm (accessed Dec 23, 2014).

(45) Costa, L. D. O.; Rossin, F. M. Optimizing the On Board Diagnostic System (OBD) to Monitor for Reduction of the SCR Catalyst Conversion Efficiency using the NOx Sensor. *SAE Tech. Pap. 2010-36-0198* **2010**.

(46) Federal Register. Control of Air Pollution From Motor Vehicles: Tier 3 Motor Vehicle Emission and Fuel Standards; Final Rule. **2014**, *79* (81), 1–474.

(47) Society of Automotive Engineers. J1939-21 Data link Layer. *SAE Int.* **2006**.

(48) O'Keefe, M. P.; Simpson, A.; Kelly, K. J.; Pedersen, D. S. Duty Cycle Characterization and Evaluation Towards Heavy Hybrid Vehicle Applications. *SAE Tech. Pap. 2007-01-0302* **2007**.

(49) Silva, C.; Ross, M.; Farias, T. Evaluation of energy consumption, emissions and cost of plug-in hybrid vehicles. *Energy Convers. Manag.* **2009**, *50* (7), 1635–1643.

(50) Manzie, C.; Watson, H.; Halgamuge, S. Fuel economy improvements for urban driving: Hybrid vs. intelligent vehicles. *Transp. Res. Part C Emerg. Technol.* **2007**, *15* (1), 1–16.

(51) Muta, K.; Yamazaki, M.; Tokieda, J. Development of new-generation hybrid system THS II - Drastic improvement of power performance and fuel economy. *2004 SAE*

World Congr. **2004**, *2004* (724), 2004-01–0064.

(52) Lukic, S. M.; Emadi, A. Effects of drivetrain hybridization on fuel economy and dynamic performance of parallel hybrid electric vehicles. *IEEE Trans. Veh. Technol.* **2004**, *53* (2), 385–389.

(53) Fontaras, G.; Pistikopoulos, P.; Samaras, Z. Experimental evaluation of hybrid vehicle fuel economy and pollutant emissions over real-world simulation driving cycles. *Atmos. Environ.* **2008**, *42* (18), 4023–4035.

(54) Johnson, V. H. Fuel Used for Vehicle Air Conditioning: A State-by-State Thermal Comfort-Based Approach. *Soc. Automot. Eng. Inc.* **2002**, *1* (724), 1957–1970.

(55) Shojaei, S.; Robinson, S.; Chatham, C.; McGordon, A.; Marco, J. Modelling the Electric Air Conditioning System in a Commercially Available Vehicle for Energy Management Optimisation. *SAE Int. 2015-01-0331* **2015**.

(56) Redfield, J.; Surampudi, B.; Gustavo, R.; Montemayor, A.; McKee, H.; Edwards, T.; Lasecki, M. Accessory Electrification in Class 8 Tractors. *SAE Tech. Pap.* **2006**, *2006* (724).

(57) Chu, X. *A Guidebook for Using Automatic Passenger Counter Data for National Transit Database (NTD) Reporting*; Tallahassee, FL, 2010.

(58) Boyle, D. *TCRP Synthesis 77 Passenger Counting Systems*; Transportation Cooperative Research Program: Washington, DC, 2008.

(59) Nassir, N.; Khani, A.; Lee, S. G.; Noh, H.; Hickman, M. Transit Stop-Level Origin-Destination Estimation Through Use of Transit Schedule and Automated Data

Collection System. *Transp. Res. Rec. J. Transp. Res. Board* **2011**, *2263* (1), 140–150.

(60) Diab, E. I.; El-geneidy, A. M. Transitory optimism : Changes in passenger perception following bus service improvement over time. *Transp. Res. Rec. J. Transp. Res. Board* **2013**, No. July, 1–20.

(61) IRISYS. Gazelle™ intelligent analytics platform for professional people counting http://www.irisys.co.uk/people-counting/products/gazelle/.

(62) Mathews, E.; Poigné, A. Using Wireless Sensor Networks. *Intell. Solut. Embed. Syst. 2008 Int. Work.* **2008**, 1–14.

(63) Slavin, C.; Feng, W.; Figliozzi, M.; Koonce, P. A Statistical Study of the Impacts of SCATS Adaptive Traffic Signal Control on Traffic and Transit Performance. *Transp. Res. Rec. J. Transp. Res. Board* **2012**.

(64) Kuutti, J. A Test Setup for Comparison of People Flow Sensors, Aalto University, 2012.

(65) Strathman, J.; Kimpel, T.; Callas, S. Validation and sampling of automatic rail passenger counters for national transit database and internal reporting at TriMet. *... J. Transp. ...* **2002**, 217–222.

(66) Trapeze Group. Intelligent Transportation Systems, Automatic Passenger Coungting. 2013, pp 1–2.

(67) Greneker, E. I.; Murphy, K.; Johnson, B.; Rausch, E. O. *Improved Passenger Counter and Classification System for Transit Operations*; Marietta, GA, 1996.

(68) Bauer, D.; Ray, M.; Seer, S. Simple Sensors Used for Measuring Service Times and Counting Pedestrians. *Transp. Res. Rec. J. Transp. Res. Board* **2011**, *2214* (1), 77–84.

(69) Peterson, D. *Effortless Passenger Identification System*; Washington, DC, 2013.

(70) Oberli, C.; Torres-torriti, M.; Landau, D. Performace Evaluation of UHF RFID Technologies for Real-Time Passenger Recognition in Intelligent Public Transport Systems. *IEEE Transctions Intell. Transp. Syst.* **2010**, *11* (3), 748–753.

(71) Gieck, J.; Society of Automotive Engineers. *Riding on Air - A History of Air Suspension*; Warrendale, PA, 1999.

(72) Krishnan, S. R.; Seelamantula, C. S. On the Selection of Optimum Savitzky-Golay Filters. *IEEE Trans.* **2013**, *61* (2), 380–391.

(73) McDowell, M. A.; Fryar, C. D.; Ogden, C. L.; Flegal, K. M. Anthropometric reference data for children and adults: United States, 2003-2006. *Natl. Health Stat. Report.* **2008**, No. 10, 1–45.

(74) Gouge, B.; Ries, F.; Dowlatabadi, H. The spatial distribution of diesel transit bus emissions and people: implications of scale on exposure and impact assessment. *Environ. Sci. Technol.* **2010**, *44* (18), 6.

(75) U.S. Government Publishing Office. *40 CFR Ch. I Section 86.007-11*; U.S. Government Publishing Office: United States, 2013; pp 228–232.

(76) Dembski, N.; Guezennec, Y.; Soliman, A. Analysis and Experimental Refinement of Real-World Driving Cycles. *SAE Tech. Pap. 2002-01-0069* **2002**, No. 724.

(77) U.S. Government Publishing Office. *40 CFR Ch. I Section 86.1370–2007*; U.S. Government Publishing Office: United States, 2012; pp 244–250.

(78) Zhan, R.; Eakle, S. T.; Miller, J. W.; Anthony, J. W. EGR System Fouling Control. *SAE Int. J. Engines* **2009**, *1* (1), 59–64.

(79) Block, M.; Clark, N.; Wayne, S.; Nine, R.; Miller, W. An Investigation into the Emissions Reduction Performance of an SCR System Over Two Years ' In-Use Heavy-Duty Vehicle Operation. *SAE Tech. Pap. 2005-01-1861* **2005**.

(80) Lammert, M. P.; McCormick, R. L.; Sindler, P.; Williams, A. Effect of B20 and Low Aromatic Diesel on Transit Bus NO x Emissions Over Driving Cycles with a Range of Kinetic Intensity. *SAE Int.* **2012**, 1–15.

(81) Andreae, M.; Salemme, G.; Kumar, M.; Sun, Z. Emissions Certification Vehicle Cycles Based on Heavy Duty Engine Test Cycles. *SAE Int. 2012-01-0878* **2012**, 299–309.

(82) Carslaw, D. C.; Beevers, S. D.; Tate, J. E.; Westmoreland, E. J.; Williams, M. L. Recent evidence concerning higher NOx emissions from passenger cars and light duty vehicles. *Atmos. Environ.* **2011**, *45* (39), 7053–7063.

(83) Velders, G. J. M.; Geilenkirchen, G. P.; de Lange, R. Higher than expected NOx emission from trucks may affect attainability of NO2 limit values in the Netherlands. *Atmos. Environ.* **2011**, *45* (18), 3025–3033.

(84) Russell, A. R.; Valin, L. C.; Bucsela, E. J.; Wenig, M. O.; Cohen, R. C. Space-based Constraints on Spatial and Temporal Patterns of NO x Emissions in California , 2005

- 2008. *Environ. Sci. Technol.* **2010**, *44* (9), 3608–3615.

(85) Anderson, K.; Ellickson, K.; Fenlon, D.; Gavin, K.; McCourtney, M.; McMahon, C.; Strassman, R.; Williams, M. *Annual Air Monitoring Network Plan for Minnesota 2016*; aq10-13a; St. Paul, MN, 2015.

(86) Tan, Y.; Lipsky, E. M.; Saleh, R.; Robinson, A. L.; Presto, A. A. Characterizing the Spatial Variation of Air Pollutants and the Contributions of High Emitting Vehicles in Pittsburgh, PA. *Environ. Sci. Technol.* **2014**, *48* (24), 14186–14194.

(87) Gately, C. K.; Hutyra, L. R.; Wing, I. S.; Brondfield, M. N. A bottom up approach to on-road CO2 emissions estimates: Improved spatial accuracy and applications for regional planning. *Environ. Sci. Technol.* **2013**, *47* (5), 2423–2430.

(88) Guttikunda, S. K.; Calori, G. A GIS based emissions inventory at 1 km by 1 km spatial resolution for air pollution analysis in Delhi, India. *Atmos. Environ.* **2013**, *67*, 101–111.

(89) Gould, G. M.; Niemeier, D. a. Spatial assignment of emissions using a new locomotive emissions model. *Environ. Sci. Technol.* **2011**, *45* (13), 5846–5852.

(90) Unal, A.; Frey, H. C.; Rouphail, N. M. Quantification of highway vehicle emissions hot spots based upon on-board measurements. *J. Air Waste Manag. Assoc.* **2004**, *54* (2), 130–140.

(91) U.S. Environmental Protection Agency. *Regulations Requiring Onboard Diagnostic Systems on 2010 and Later Heavy-Duty Engines Used in Highway Vehicles Over 14,000 Pounds; Revisions to Onboard Diagnostics Requirements for Diesel*

Highway Vehicles Under 14,000 Pounds; EPA420-R-08-019; 2008.

(92) Penney, G. P.; Weese, J.; Little, J. a; Desmedt, P.; Hill, D. L.; Hawkes, D. J. A comparison of similarity measures for use in 2-D-3-D medical image registration. *IEEE Trans. Med. Imaging* **1998**, *17* (4), 586–595.

(93) Pant, A.; Schmieg, S. J. Kinetic model of NOx SCR using urea on commercial Cu-zeolite catalyst. *Ind. Eng. Chem. Res.* **2011**, *50*, 5490–5498.

(94) Federal Highway Administration. *Annual Vehicle Distance Traveled in Miles and Related Data - 2012*; Table VM-1; 2014.

(95) Niemeier, D. a. Spatial applicability of emission factors for modeling mobile emissions. *Environ. Sci. Technol.* **2002**, *36* (4), 736–741.

(96) Misra, C.; Collins, J. F.; Herner, J. D.; Sax, T.; Krishnamurthy, M.; Sobieralski, W.; Burntizki, M.; Chernich, D. In-Use NOx Emissions from Model Year 2010 and 2011 Heavy-Duty Diesel Engines Equipped with Aftertreatment Device. *Environ. Sci. Technol. Technol.* **2013**, *47*, 7892–7898.

(97) Aloquili, O.; Elbanna, a.; Al-Azizi, a. Automatic vehicle location tracking system based on GIS environment. *IET Softw.* **2009**, *3* (4), 255.

(98) Girard, J.; Cavataio, G.; Snow, R.; Lambert, C. Combined Fe-Cu SCR Systems with Optimized Ammonia to NOx Ratio for Diesel NOx Control. *SAE Int.J.Fuels Lubr.* **2008**, *1* (1), 603–610.

(99) Munnannur, A.; Chiruta, M.; Liu, Z. G. Thermal and Fluid Dynamic Considerations in Aftertreatment System Design for SCR Solid Deposit Mitigation. *SAE Tech. Pap.*

2012, No. 1.

(100) Herman, A.; Wu, M.-C.; Cabush, D.; Shost, M. Model Based Control of SCR Dosing and OBD Strategies with Feedback from NH 3 Sensors. *SAE Int. J. Fuels Lubr.* **2009**, *2* (1), 375–385.

(101) Narayanaswamy, K.; He, Y. Modeling of Copper-Zeolite and Iron-Zeolite Selective Catalytic Reduction (SCR) Catalysts at Steady State and Transient Conditions. *SAE Int. 2008-01-0615* **2008**.

(102) Koebel, M.; Elsener, M.; Kleemann, M. Urea-SCR: a promising technique to reduce NOx emissions from automotive diesel engines. *Catal. Today* **2000**, *59* (3), 335–345.

(103) Girard, J.; Snow, R.; Cavataio, G.; Lambert, C. The Influence of Ammonia to NOX Ratio on SCR Performance. *SAE Tech. Pap. 2007-01-1581* **2007**.

(104) Klingstedt, F.; Arve, K.; Murzin, D. Y. U. Toward Improved Catalytic Low-Temperature NO x Removal in Diesel-Powered Vehicles. *Acc. Chem. Res.* **2006**, *39* (4), 273–282.

(105) Koebel, M.; Elsener, M.; Madia, G. Reaction pathways in the selective catalytic reduction process with NO and NO2 at low temperatures. *Ind. Eng. Chem. Res.* **2001**, *40* (1), 52–59.

(106) Ettireddy, P. R.; Kotrba, A.; Spinks, T.; Boningari, T.; Smirniotis, P. Development of Low Temperature Selective Catalytic Reduction (SCR) Catalysts for Future Emissions Regulations. *SAE Tech. Pap. 2014-01-1520* **2014**.

(107) Kang, M.; Park, E. D.; Kim, J. M.; Yie, J. E. Cu-Mn mixed oxides for low temperature NO reduction with NH3. *Catal. Today* **2006**, *111* (3–4), 236–241.

(108) Kang, M.; Park, E. D.; Kim, J. M.; Yie, J. E. Manganese oxide catalysts for NOx reduction with NH3 at low temperatures. *Appl. Catal. A Gen.* **2007**, *327* (2), 261–269.

(109) Peña, D. A.; Uphade, B. S.; Smirniotis, P. G. TiO2-supported metal oxide catalysts for low-temperature selective catalytic reduction of NO with NH3: I. Evaluation and characterization of first row transition metals. *J. Catal.* **2004**, *221* (2), 421–431.

(110) Yoshikawa, M.; Yasutake, A.; Mochida, I. Low-temperature selective catalytic reduction of NO(x) by metal oxides supported on active carbon fibers. *Appl. Catal. a-General* **1998**, *173* (2), 239–245.

(111) Tang, X.; Hao, J.; Yi, H.; Li, J. Low-temperature SCR of NO with NH3 over AC/C supported manganese-based monolithic catalysts. *Catal. Today* **2007**, *126* (3–4 SPEC. ISS.), 406–411.

(112) Chi, J. N.; Dacosta, H. F. M. Modeling and Control of a Urea-SCR Aftertreatment System Reprinted From : Diesel Exhaust Emission Control Modeling. *SAE Tech. Pap. 2005-01-0966* **2005**, *114* (4), 449–464.

(113) Chavannavar, P. Development and Implementation of a Mapless, Model Based SCR Control System. *SAE Int. J. Engines* **2014**, *7* (2), 1113–1124.

(114) Muncrief, R. L.; Rooks, C. W.; Cruz, M.; Harold, M. P. Combining Biodiesel and Exhaust Gas Recirculation for Reduction in NOx and Particulate Emissions. *Energy*

and Fuels **2008**, *22* (2), 1285–1296.

(115) Johnson, D. R.; Bedick, C. R.; Clark, N. N.; Mckain, D. L. Design and testing of an independently controlled urea SCR retrofit system for the reduction of NOx emissions from marine diesels. *Environ. Sci. Technol.* **2009**, *43* (10), 3959–3963.

(116) Herner, J. D.; Hu, S.; Robertson, W. H.; Huai, T.; Chang, M. C. O.; Rieger, P.; Ayala, A. Effect of advanced aftertreatment for PM and NOx reduction on heavy-duty diesel engine ultrafine particle emissions. *Environ. Sci. Technol.* **2011**, *45* (6), 2413–2419.

(117) Herner, J. D.; Hu, S.; Robertson, W. H.; Huai, T.; Collins, J. F.; Dwyer, H.; Ayala, A. Effect of advanced aftertreatment for PM and NOx control on heavy-duty diesel truck emissions. *Environ. Sci. Technol.* **2009**, *43* (15), 5928–5933.

(118) Yao, C.; Cheung, C. S.; Cheng, C.; Wang, Y. Reduction of smoke and NOx from diesel engines using a diesel/methanol compound combustion system. *Energy and Fuels* **2007**, *21* (2), 686–691.

(119) Jeon, J.; Lee, J. T.; Park, S. Nitrogen Compounds (NO, NO2 , N2O, and NH3) in NOx Emissions from Commercial EURO VI Type Heavy-Duty Diesel Engines with a Urea-Selective Catalytic Reduction System. *Energy & Fuels* **2016**, *30* (8), 6828–6834.

(120) Kotz, A. J.; Kittelson, D. B.; Northrop, W. F. Lagrangian Hotspots of In-Use NOx Emissions from Transit Buses. *Environ. Sci. Technol.* **2016**, *50* (11), 5750–5756.

(121) Posada, F.; Bandivadekar, A. Global overview of on-board diagnostic (OBD)

systems for heavy-duty vehicles http://www.theicct.org/sites/default/files/publications/ICCT_Overview_OBD-HDVs_20150209.pdf.

(122) Stanton, D. W. Systematic Development of Highly Efficient and Clean Engines to Meet Future Commercial Vehicle Greenhouse Gas Regulations. *SAE Int. 2013-01-2421* **2013**.

(123) Zhang, H.; Wang, J.; Wang, Y.-Y. Removal of NOx sensor ammonia cross sensitivity from contaminated measurements in Diesel-engine selective catalytic reduction systems. *Fuel* **2015**, *150*, 448–456.

(124) Zhang, H.; Wang, J. NOx Sensor Ammonia-Cross-Sensitivity Factor Estimation in Diesel Engine Selective Catalytic Reduction Systems. *J. Dyn. Syst. Meas. Control* **2015**, *137* (6), 61015.

(125) Hsieh, M.-F. Control of Diesel Engine Urea Selective Catalytic Reduction Systems, 2010.

(126) Society of Automotive Engineers. J1939-71 Vehicle Application layer. *SAE Int.* **2012**, *J1939-71*.

(127) Birkhold, F.; Meingast, U.; Wassermann, P. Analysis of the Injection of Urea-Water-Solution for Automotive SCR DeNOx-Systems : Modeling of Two-Phase Flow and Spray / Wall-Interaction Reprinted From : Diesel Exhaust. *SAE Int.* **2006**, *2006-01–06*.

(128) DieselNet. Emissions Standards - Heavy Duty Onroad Engines

https://www.dieselnet.com/standards/us/hd.php#stds (accessed Oct 4, 2016).

(129) Gunturi, V. M. V; Nunes, E.; Yang, K.; Shekhar, S. A Critical-Time-Point Approach to All-Start-Time Lagrangian Shortest Paths: A Summary of Results. *Adv. Spat. Temporal Databases* **2011**, *6849*, 74–91.

(130) Gunturi, V. M. V; Shekhar, S. Lagrangian Xgraphs: A Logical Data-Model for Spatio-Temporal Network Data: A Summary. *Adv. Concept. Model.* **2014**, *8823*, 201–211.

(131) Ali, R. Y.; Gunturi, V. M. V; Shekhar, S.; Eldawy, A.; Mokbel, M. F.; Kotz, A. J.; Northrop, W. F. Future Connected Vehicles : Challenges and Opportunities for Spatio-temporal Computing (Vision Paper). *ACM Int. Conf. Adv. Geogr. Inf. Syst.* **2015**, No. Article No. 14, 20–23.

(132) Ali, R. Y.; Gunturi, V. M. V; Kotz, A. J.; Shekhar, S.; Northrop, W. F. Discovering Non-compliant Window Co-Occurrence Patterns: A Summary of Results. *Adv. Spat. Temporal Databases* **2015**, *9239*, 391–410.